

# 1 Evaluation and uncertainty investigation of the NO<sub>2</sub>, CO and NH<sub>3</sub> 2 modeling over China under the framework of MICS-Asia III

3 Lei Kong<sup>1,3</sup>, Xiao Tang<sup>2,3</sup>, Jiang Zhu<sup>1,3</sup>, Zifa Wang<sup>2,3</sup>, Joshua S. Fu<sup>4</sup>, Xuemei Wang<sup>5</sup>, Syuichi Itahashi<sup>6,7</sup>,  
4 Kazuyo Yamaji<sup>8</sup>, Tatsuya Nagashima<sup>9</sup>, Hyo-Jung Lee<sup>10</sup>, Cheol-Hee Kim<sup>10</sup>, Chuan-Yao Lin<sup>11</sup>, Lei Chen<sup>2,3</sup>,  
5 Meigen Zhang<sup>2,3</sup>, Zhining Tao<sup>12,13</sup>, Jie Li<sup>2,3</sup>, Mizuo Kajino<sup>14,15</sup>, Hong Liao<sup>16</sup>, Zhe Wang<sup>17,2</sup>, Kengo Sudo<sup>18</sup>,  
6 Yuesi Wang<sup>2,3</sup>, Yuepeng Pan<sup>2,3</sup>, Guiqian Tang<sup>2,3</sup>, Meng Li<sup>19,20</sup>, Qizhong Wu<sup>21,22</sup>, Baozhu Ge<sup>2,3</sup>, Gregory  
7 R. Carmichael<sup>23</sup>

8 <sup>1</sup>ICCES, Institute of Atmospheric Physics, Chinese Academy of Sciences, Beijing, 100029, China

9 <sup>2</sup>LAPC, Institute of Atmospheric Physics, Chinese Academy of Sciences, Beijing, 100029, China

10 <sup>3</sup>University of Chinese Academy of Sciences, Beijing, 100049, China

11 <sup>4</sup>Department of Civil and Environmental Engineering, University of Tennessee, Knoxville, TN, 37996, USA

12 <sup>5</sup>Institute for Environment and Climate Research, Jinan University, Guangzhou, 510632, China

13 <sup>6</sup>Central Research Institute of Electric Power Industry, Abiko, Chiba, 270-1194, Japan

14 <sup>7</sup>Department of Marine, Earth, and Atmospheric Sciences, North Carolina State University, Raleigh, NC 27607, USA

15 <sup>8</sup>Graduate School of Maritime Sciences, Kobe University, Kobe, Hyogo 658-0022, Japan

16 <sup>9</sup>National Institute for Environmental Studies, Onogawa, Tsukuba 305-8506, Japan

17 <sup>10</sup>Department of Atmospheric Sciences, Pusan National University, Busan, 46241, South Korea

18 <sup>11</sup>Research Center for Environmental Changes, Academia Sinica, Taipei, 115, Taiwan

19 <sup>12</sup>Universities Space Research Association, Columbia, MD, USA

20 <sup>13</sup>NASA Goddard Space Flight Center, Greenbelt, MD, 130, USA

21 <sup>14</sup>Meteorological Research Institute, Japan Meteorological Agency, Tsukuba, Ibaraki, 305-0052, Japan

22 <sup>15</sup>Faculty of Life and Environmental Sciences, University of Tsukuba, Tsukuba, Ibaraki, 305-8577, Japan

23 <sup>16</sup>Jiangsu Key Laboratory of Atmospheric Environment Monitoring and Pollution Control, Collaborative Innovation Center of  
24 Atmospheric Environment and Equipment Technology, School of Environmental Science and Engineering, Nanjing  
25 University of Information Science and Technology, Nanjing 210044, China

26 <sup>17</sup>Research Institute for Applied Mechanics (RIAM), Kyushu University, Fukuoka, Japan

27 <sup>18</sup>Graduate School of Environmental Studies, Nagoya University, Nagoya, Japan

28 <sup>19</sup>Ministry of Education Key laboratory for Earth System Modeling, Department of Earth System Science, Tsinghua University,  
29 Beijing, 100084, China

30 <sup>20</sup>Multiphase Chemistry Department, Max Planck Institute for Chemistry, Mainz, 55128, Germany

31 <sup>21</sup>College of Global Change and Earth System Science, Beijing Normal University, Beijing 100875, China

32 <sup>22</sup>Joint Centre for Global Changes Studies, Beijing Normal University, Beijing 100875, China

33 <sup>23</sup>Center for Global and Regional Environmental Research, University of Iowa, Iowa City, IA, 52242, USA

34 *Correspondence to:* Xiao Tang([tangxiao@mail.iap.ac.cn](mailto:tangxiao@mail.iap.ac.cn))

35 **Abstract.** Despite the significant progress in improving the chemical transport models (CTMs), applications of these modeling  
36 endeavours are still subject to the large and complex model uncertainty. Model Inter-Comparison Study for Asia III (MICS-  
37 Asia III) has provided the opportunity to assess the capability and uncertainty of current CTMs in East Asia applications. In  
38 this study, we have evaluated the multi-model simulations of nitrogen dioxide (NO<sub>2</sub>), carbon monoxide (CO) and ammonia  
39 (NH<sub>3</sub>) over China under the framework of MICS-Asia III. Thirteen modeling results, provided by several independent groups  
40 from different countries/regions, were used in this study. Most of these models used some modeling domain with a horizontal

41 resolution of 45km, and were driven by common emission inventories and meteorological inputs. New observations over North  
42 China Plain (NCP) and Pearl River Delta (PRD) regions were also available in MICS-Asia III, allowing the model evaluations  
43 over highly industrialized regions. The evaluation results show that most models well captured the monthly and spatial patterns  
44 of NO<sub>2</sub> concentrations in the NCP region though NO<sub>2</sub> levels were slightly underestimated. Relatively poor performance in  
45 NO<sub>2</sub> simulations was found in the PRD region with larger root mean square error and lower spatial correlation coefficients,  
46 which may be related to the coarse resolution or inappropriate spatial allocations of the emission inventories in the PRD region.  
47 All models significantly underpredicted CO concentrations in both the NCP and PRD regions, with annual mean concentrations  
48 65.4% and 61.4% underestimated by the ensemble mean. Such large underestimations suggest that CO emissions might be  
49 underestimated in current emission inventory. In contrast to the good skills in simulating the monthly variations of NO<sub>2</sub> and  
50 CO concentrations, all models failed to reproduce the observed monthly variations of NH<sub>3</sub> concentrations in the NCP region.  
51 Most models mismatched the observed peak in July and showed negative correlation coefficients with the observations, which  
52 may be closely related to the uncertainty in the monthly variations of NH<sub>3</sub> emissions and the NH<sub>3</sub> gas-aerosol partitioning.  
53 Finally, model inter-comparisons have been conducted to quantify the impacts of model uncertainty on the simulations of these  
54 gases which are shown increase with the reactivity of species. Models contained more uncertainty in the NH<sub>3</sub> simulations. This  
55 suggests that for some highly active and/or short-lived primary pollutants, like NH<sub>3</sub>, model uncertainty can also take a great  
56 part in the forecast uncertainty besides the emission uncertainty. Based on these results, some recommendations are made for  
57 future studies.

## 58 **1 Introduction**

59 As the rapid growth in East Asia's economy with surging energy consumption and emissions, air pollution has become  
60 an increasingly important scientific topic and political concern in East Asia due to its significant environmental and health  
61 effects (Anenberg et al., 2010;Lelieveld et al., 2015). Chemical transport models (CTMs), serving as a critical tool in both the  
62 scientific research and policy makings, have been applied into various air quality issues, such as air quality prediction, long-  
63 range transport of atmospheric pollutants, development of emission control strategies and understanding of observed chemical  
64 phenomena (e.g. Cheng et al., 2016;Li et al., 2017a;Lu et al., 2017;Ma et al., 2019;Tang et al., 2011;Xu et al., 2019;Zhang et  
65 al., 2019). Nevertheless, air quality modeling remains a challenge due to the multi-scale and non-linear nature of the complex  
66 atmospheric processes (Carmichael et al., 2008). It still suffers from large uncertainties related to the missing or poorly  
67 parameterized physical and chemical processes, inaccurate and/or incomplete emission inventories as well as the poorly  
68 represented initial and boundary conditions (Carmichael et al., 2008;Dabberdt and Miller, 2000;Fine et al., 2003;Gao et al.,  
69 1996;Mallet and Sportisse, 2006). Understanding such uncertainties and their impacts on the air quality modeling is of great  
70 importance in assessing the robustness of models for their applications in scientific research and operational use.

71 There are specific techniques to assess these uncertainties. Monte Carlo simulations, based on different values of model  
72 parameters or input fields sampled from a predefined probability density function (PDF), can provide an approximation to the

73 PDF of possible model output and serves as an excellent characterization of the uncertainties in simulations (Hanna et al.,  
74 2001). However, this method is more suited to deal with the uncertainty related to the continuous variables, such as input data  
75 or parameters in parameterization. The ensemble method, based on a set of different models, is an alternative approach to  
76 accounting for the range of uncertainties (Galmarini et al., 2004; Mallet and Sportisse, 2006). For example, the Air Quality  
77 Model Evaluation International Initiative (AQMEII) has been implemented in Europe and North America to investigate the  
78 model uncertainties of their regional-scale model predictions (Rao et al., 2011). To assess the model performances and  
79 uncertainties in East Asia applications, the Model Inter-Comparison Study for Asia (MICS-Asia) has been initiated in year  
80 1998. The first Phase of MICS-Asia (MICS-Asia I) was carried out during period 1998–2002, mainly focusing on the long-  
81 range transport and depositions of sulfur in Asia (Carmichael et al., 2002). In 2003, the second phase (MICS-Asia II) was  
82 initiated and took more species related to the regional health and ecosystem protection into account, including nitrogen  
83 compounds, O<sub>3</sub> and aerosols. Launched in 2010, MICS-Asia III has greatly expanded its study scope by covering three  
84 individual and interrelated topics: (1) evaluate strength and weaknesses of current multi-scale air quality models and provide  
85 techniques to reduce uncertainty in Asia; (2) develop a reliable anthropogenic emission inventories in Asia and understanding  
86 uncertainty of bottom-up emission inventories in Asia; (3) provide multi-model estimates of radiative forcing and sensitivity  
87 analysis of short-lived climate pollutants.

88 This study addresses one component of topic 1, focusing on the three gas pollutants of NO<sub>2</sub>, CO and NH<sub>3</sub>. Compared with  
89 MICS-Asia II, more modeling results (fourteen different models with thirteen regional models and one global model) were  
90 brought together within the topic 1 of MICS-Asia III, run by independent modeling groups from China, Japan, Korea, United  
91 States of America and other countries/regions. The different models contain differences in their numerical approximations  
92 (time step, chemical solver, etc.) and parameterizations, which represent a sampling of uncertainties residing in the air quality  
93 modeling. However, it would be difficult to interpret the results from inter-comparison studies when the models were driven  
94 by different meteorological fields and emission inventories. Thus, in MICS-Asia III the models were constrained to be operated  
95 under the same conditions by using the common emission inventories, meteorological fields, modeling domain and horizontal  
96 resolutions. The simulations were also extended from the four months in MICS-Asia II to one-full year of 2010.

97 NO<sub>2</sub>, CO and NH<sub>3</sub> are three important primary gas pollutants that has wide impacts on the atmospheric chemistry. As a  
98 major precursor of O<sub>3</sub>, NO<sub>2</sub> plays an important role in the tropospheric O<sub>3</sub> chemistry, and also contributes to the rainwater  
99 acidification and the formation of secondary aerosols (Dentener and Crutzen, 1993; Evans and Jacob, 2005). CO is a colorless  
100 and toxic gas ubiquitous throughout the atmosphere which is of interest as an indirect greenhouse gas (Gillenwater, 2008) and  
101 a precursor for tropospheric O<sub>3</sub> (Steinfeld, 1998). Being the major sink of OH, CO also controls the atmosphere's oxidizing  
102 capacity (Levy, 1971; Novelli et al., 1998). As the only primary alkaline gas in the atmosphere, NH<sub>3</sub> is closely associated with  
103 the acidity of precipitations for one thing, for another it can react with sulfuric acid and nitric acid forming ammonium sulfate  
104 and ammonium nitrate which account for a large proportion of fine particulate matter (Sun et al., 2012; Sun et al., 2013).  
105 Assessing their model performances is thus important to help us better understand their environmental consequences and also  
106 help explain the model performances for their related secondary air pollutants, such as O<sub>3</sub> and fine particulate matter.

107 In previous phase of MICS-Asia, no specific evaluation and inter-comparison work has been conducted for these gases,  
108 especially for CO and NH<sub>3</sub>. In MICS-Asia II, model performance of NO<sub>2</sub> was evaluated as a relevant species to O<sub>3</sub> (Han et al.,  
109 2008b), however such evaluations were limited to the observation sites from EANET (Acid Deposition Monitoring Network  
110 in East Asia). Model evaluations and inter-comparisons in industrialized regions of China has not been performed due to the  
111 limited number of monitoring sites in China from EANET, which hindered our understanding of the model performance in  
112 industrialized regions. More densely observations over highly industrialized regions of China, namely the North China (NCP)  
113 Plain and Pearl River Delta (PRD) regions, were first included in MICS-Asia III, allowing the model evaluations over highly  
114 industrialized regions. Meanwhile, the emission inventories of these three gases still subject to the large uncertainties  
115 (Kurokawa et al., 2013;Li et al., 2017b), which is a major source of uncertainties in air quality modeling and forecast.  
116 Evaluating these gases' emission inventories from a model perspective is also a useful way to identify the uncertainties in  
117 emission inventories (Han et al., 2008a;Noije et al., 2006;Pinder et al., 2006;Stein et al., 2014;Uno et al., 2007).

118 In all, this paper is aimed at evaluating the NO<sub>2</sub>, CO and NH<sub>3</sub> simulations using the multi-model data from MICS-Asia  
119 III, three questions are trying to be addressed: (1) what is the performance of current CTMs in simulating the NO<sub>2</sub>, CO and  
120 NH<sub>3</sub> concentrations over highly industrialized regions of China, (2) what are the potential factors responsible for the model  
121 deviations from observations and differences among models, and (3) how large are the impacts of model uncertainties on the  
122 simulations of these gases.

## 123 **2 Inter-comparison frameworks**

### 124 **2.1 Description on the participating models and input datasets**

125 Six different chemical transport models have participated in MICS-Asia III with their major configurations summarized  
126 in Table 1. These models included NAQPMS (Wang et al., 2001), three versions of CMAQ (Byun and Schere, 2006), WRF-  
127 Chem (Grell et al., 2005), NU-WRF (Peters-Lidard et al., 2015), NHM-Chem (Kajino et al., 2012) and GEOS-Chem  
128 (<http://acmg.seas.harvard.edu/geos/>). All models employed a same modeling domain (Fig. 1) with a horizontal resolution of  
129 45km except M13 (0.5° of latitude×0.667° of longitude) and M14 (64km×64km). Detailed information on each component of  
130 these CTMs can be obtained from the companion paper by Chen et al., 2019 and Tan et al., 2019.

131 Standard model input datasets of raw meteorological fields, emission inventory and boundary conditions were provided  
132 by MICS-Asia III for all participants. Raw meteorological fields were generated from a whole year simulations of 2010 using  
133 Weather Research and Forecasting Model (WRF) version 3.4.1 (Skamarock, 2008) with horizontal resolution of 45km and  
134 vertically 40 layers from surface to the model top (10hPa). Initial and lateral boundary conditions for meteorological simulation  
135 were generated every six hours by using the 1°×1° NCEP FNL (Final) Operational Global Analysis data (ds083.2). Real-time,  
136 global, sea surface temperature (RTG\_SST\_HR) analysis were used to generate and update lower boundary conditions for sea  
137 areas. Four-dimensional data assimilation nudging (Gridded FDDA & SFDDA) was performed during the simulation to  
138 increase the accuracy of WRF after the objective analysis with NCEP FNL (Final) Operational Global Analysis data (ds083.2),

139 NCEP ADP Global Surface Observation Weather Data (ds461.0) and NCEP ADP Global Upper Air and Surface Weather Data  
140 (ds337.0). Detailed configurations of the standard meteorological model are available in supplementary Table S1. The  
141 simulated wind speed, relative humidity and air temperature were evaluated against the observations over the NCP and PRD  
142 regions with detailed results shown in supplementary Sect. S1. In general, the standard meteorological simulations well  
143 captured the main features of meteorological conditions in the NCP and PRD regions with high correlation coefficient, small  
144 biases and low errors for all meteorological parameters (supplementary Fig.S1-S3 and Table S2).

145 Standard emission inventories provided by the MICS-Asia III were used by all participants. The anthropogenic emissions  
146 were provided by a newly developed anthropogenic emission inventory for Asia (MIX) which integrated five national or  
147 regional inventories, including Regional Emission inventory in Asia (REAS) inventory for Asia developed at the Japan  
148 National Institute for Environment Studies, the Multi-resolution Emission Inventory for China (MEIC) developed at Tsinghua  
149 University, the high-resolution ammonia emission inventory in China developed at Peking University, the Indian emission  
150 inventory developed at Argonne National Laboratory in the United States, and the Clean Air Policy Support System (CAPSS)  
151 Korean emission inventory developed at Konkuk University (Li et al., 2017b). Hourly biogenic emissions for the entire year  
152 of 2010 in MICS-Asia III were provided by the Model of Emissions of Gases and Aerosols from Nature version 2.04 (Guenther  
153 et al., 2006). The Global Fire Emissions Database 3 (Randerson et al., 2013) was used for biomass burning emissions. Volcanic  
154 SO<sub>2</sub> emissions were provided by the Asia Center for Air Pollution Research (ACAP) with a daily temporal resolution. Air and  
155 ship emissions with an annual resolution were provided by the HTAPv2 emission inventory for 2010 (Janssens-Maenhout et  
156 al., 2015). NMVOC emissions were spectated into the model-ready inputs for three chemical mechanisms: CBMZ, CB05 and  
157 SAPRC-99 and the weekly and diurnal profiles for emissions were also provided.

158 MICS-Asia III has provided two sets of top and lateral boundary conditions for year 2010, which were derived from the  
159 3-hourly global CTM outputs of CHASER (Sudo et al., 2002a; Sudo et at., 2002b) and GEOS-Chem  
160 (<http://acmg.seas.harvard.edu/geos/>), run by Nagoya University (Japan) and the University of Tennessee (USA) respectively.  
161 GEOS-Chem was run with 2.5°×2° resolution and 47 vertical layers while CHASER model was run with 2.8°×2.8° and 32  
162 vertical layers.

163 All participants were required to use the standard model input data to drive their model run so that the impacts of model  
164 input data on simulations could be minimized. However, models are quite different from each other, and it is difficult to keep  
165 all the inputs the same. The majority of models have applied the standard meteorology fields, while the GEOS-Chem and  
166 RAMS-CMAQ utilized their own meteorology models. The GEOS-Chem was driven by the GEOS-5 assimilated  
167 meteorological fields from the Goddard Earth Observing System of the NASA Global Modeling Assimilation Office, and the  
168 RAMS-CMAQ was driven by meteorological fields provided by Regional Atmospheric Modeling System (RAMS) (Pielke et  
169 al., 1992). WRF-Chem utilized the same meteorology model (WRF) as the standard meteorological simulation, but two of  
170 them considered the two-way coupling effects of pollutants and meteorological fields. The meteorological configurations of  
171 these WRF-Chem models were compared to the configurations of the standard meteorological model (supplementary table  
172 S1), which shows slight differences from the standard meteorological model. The CTM part of NHM-Chem is coupled with

173 the JMA's non-hydrostatic meteorological model (NHM) (Saito et al., 2006), but an interface to convert a meteorological  
174 model output of WRF to a CTM input was implemented (Kajino et al., 2018). Thus, the standard meteorology field was used  
175 in the NHM-Chem simulation, too.

## 176 **2.2 Data and statistical methods**

177 All modeling groups have performed a base year simulations of 2010 and were required to submit their modeling results  
178 according to the data protocol designed in MICS-Asia III. Gridded monthly concentrations of NO<sub>2</sub>, CO, NH<sub>3</sub> and ammonium  
179 (NH<sub>4</sub><sup>+</sup>) in the surface layer were used in this study. Note that modeling results from M3 and NH<sub>3</sub> simulations from M8 were  
180 excluded due to their incredible results, thus only thirteen modeling results were used in this study.

181 Hourly observed concentrations of NO<sub>2</sub> and CO were collected over the NCP (19 stations) and PRD (13 stations) regions,  
182 obtained from the air quality network over North China (Tang et al., 2012) and the Pearl River Delta regional air quality  
183 monitoring network (PRD RAQMN), respectively. The air quality monitoring network over North China was set up by the  
184 Chinese Ecosystem Research Network (CERN), the Institute of Atmospheric Physics (IAP) and the Chinese Academy of  
185 Sciences (CAS) since 2009 within an area of 500×500 km<sup>2</sup> in northern China. All monitoring stations were selected and set  
186 up according to the US EPA method designations (Ji et al., 2012). The PRD RAQMN network was jointly established by the  
187 government of the Guangdong Province and the Hong Kong Special Administrative Region, consisting of 16 automatic air  
188 quality monitoring stations across the PRD region (Zhong et al., 2013). Thirteen of these stations are operated by the  
189 Environmental Monitoring Centers in the Guangdong Province which were used in this study, while the other three are located  
190 in Hong Kong (not included in this study) and are managed by the Hong Kong Environmental Protection Department. Monthly  
191 averaged observations were calculated for the comparisons with the simulated monthly surface NO<sub>2</sub> and CO concentrations. It  
192 should be noted that these networks measured the NO<sub>2</sub> concentrations using a thermal conversion method, which would  
193 overestimate the NO<sub>2</sub> concentrations due to the positive interference of other oxidized nitrogen compounds (Xu et al., 2013).

194 NH<sub>3</sub> observations for long-term period are indeed challenging and limited due to its strong spatial and temporal variability,  
195 quick conversion from one phase to another and also its stickiness to the observational instruments (von Bobruzki et al., 2010).  
196 Measurements of surface NH<sub>3</sub> concentrations in year 2010 were not available in this study, however, one-year surface  
197 measurement of monthly NH<sub>3</sub> concentrations over China from September of 2015 to August of 2016 were used as a reference  
198 dataset in this study, which were obtained from the Ammonia Monitoring Network in China (AMoN-China) (Pan et al., 2018)  
199 The AMoN-China was established based on the CERN and the Regional Atmospheric Deposition Observation Network in  
200 North China Plain (Pan et al., 2012), which consists of 53 sites over the whole China and measured the monthly ambient NH<sub>3</sub>  
201 concentrations using the passive diffusive technique. Eleven stations located in the NCP region were used in this study.  
202 Distributions of the observation sites of NO<sub>2</sub>, CO and NH<sub>3</sub> over the NCP and PRD regions as well as their total emissions in  
203 year 2010 provided by MICS-Asia III are shown in Fig. 1. Besides the surface observations, the satellite retrievals of NH<sub>3</sub> total  
204 columns from IASI (Infrared Atmospheric Sounding Interferometer) were also used in this study to qualitatively evaluate the  
205 modeled monthly variations of NH<sub>3</sub> concentrations. The ANNI-NH3-v2.1R-I retrieval product (Van Damme et al., 2017; Van

206 Damme et al., 2018) was used in this study which is the reanalysis version of NH<sub>3</sub> retrievals from IASI instruments and  
207 provides the daily morning (~9:30 am local time) NH<sub>3</sub> total columns from year 2008 to 2016. More detailed information and  
208 the processing of satellite data are available in supplementary sect. S2.

209 Mean bias error (MBE), normalized mean bias (NMB), root mean square error (RMSE) and correlation coefficient (R)  
210 were calculated for the assessment of model performances. Standard deviation of the ensemble models was used to measure  
211 the ensemble spread and the impacts of model uncertainty. Coefficient of variation (hereinafter, CV), defined as the standard  
212 deviation divided by the average with larger value denoting lower consistency among models, was also used to measure the  
213 impacts of model uncertainty in a relative sense. However, by this definition, there is a tendency that lower concentrations are  
214 more likely associated with higher value of CV, thus we did not calculate the values of CV over model grids whose simulated  
215 concentrations were lower than 0.1 ppbv for NO<sub>2</sub> and NH<sub>3</sub>, and 0.1 ppmv for CO, respectively. March–May, Jun–August,  
216 September–November and December–February were used to define the four seasons that are spring, summer, autumn and  
217 winter, respectively.

## 218 **3 Results**

### 219 **3.1 Evaluating the ensemble models with observations**

220 To facilitate comparisons, the modeling results were interpolated to the observation sites by taking the values from the  
221 grid cell where the monitoring stations located. Model evaluation metrics defined in Sect. 2.2 were then calculated to evaluate  
222 the modeling results against the observations.

#### 223 **3.1.1 NO<sub>2</sub>**

224 Figure 2 displays the comparisons between the observed and simulated annual mean NO<sub>2</sub> concentrations over the NCP  
225 (2a) and PRD(2b) regions with calculated model evaluation metrics summarized in Table 2. M13 is not included in the  
226 evaluation of NO<sub>2</sub> since it did not submitted the NO<sub>2</sub> concentrations. In general, the majority of models underpredicted NO<sub>2</sub>  
227 levels in both the NCP and PRD regions. Calculated MBE (NMB) ranges from -6.54 ppbv (-28.4%) to -2.45 (-10.6%) ppbv  
228 over the NCP region and from -9.84 ppbv (-44.0%) to -1.84 ppbv (-8.2%) over the PRD region among these negatively-biased  
229 models. These underpredicted NO<sub>2</sub> concentrations are consistent with the overpredicted O<sub>3</sub> concentrations by these models  
230 found in the companion paper by Li et al., 2019. O<sub>3</sub> productions can either increase with NO<sub>x</sub> under NO<sub>x</sub> limited conditions or  
231 decrease under the NO<sub>x</sub> saturated (also called volatile organic compounds (VOCs) limited) conditions (Sillman, 1999). Both  
232 the NCP and PRD regions are industrialized regions in China with high NO<sub>x</sub> emissions (Fig. 1). Observations also showed that  
233 the NCP and PRD regions are falling into or changing into the NO<sub>x</sub> saturated regimes (Shao et al., 2009; Jin and Holloway,  
234 2015). Therefore, the underestimated NO<sub>2</sub> concentrations may contribute to the overpredicted O<sub>3</sub> concentrations in these two  
235 regions. The detailed results about the O<sub>3</sub> predictions can be found in the companion paper by Li et al., 2019. In addition, as  
236 we mentioned in Sect.2.2, the negative biases in the simulated NO<sub>2</sub> concentrations can be also partly attributed to the positive

237 biases in the NO<sub>2</sub> observations. M5, M8, M9 and M11 in the NCP region and M5, M8 and M11 in the PRD region were  
238 exceptions that overpredicted NO<sub>2</sub> concentrations. M11 showed good performances in predicting NO<sub>2</sub> levels in the NCP region  
239 with smallest RMSE, while M9 significantly overestimated NO<sub>2</sub> with largest MBE and RMSE values. NO<sub>2</sub> predictions by M8  
240 were close to the observations over the PRD region with smallest RMSE value. Meanwhile, we also found that models  
241 exhibited better NO<sub>2</sub> modeling skills in the NCP region than that in the PRD region with smaller bias and RMSE values.

242 According to the spatial correlation coefficients (Table 2), all models well reproduced the main features of the spatial  
243 variability of NO<sub>2</sub> concentrations in the NCP region with correlation coefficients ranging from 0.57 to 0.70. However, models  
244 failed in capturing the spatial variability of NO<sub>2</sub> concentrations in the PRD region with correlation coefficients only ranged  
245 from 0.00 to 0.38. Such low correlation might be attributed to the coarser model resolution (45km) that some local impacts on  
246 the NO<sub>2</sub> concentrations might not be well resolved in the model, and/or related to the uncertainties in emission inventories  
247 which were not well resolved in the PRD region. To investigate it, we have conducted an additional one-year simulation with  
248 finer horizontal resolutions (15km and 5km, supplementary Fig.S4) in the PRD region using the NAQPMS model. Detailed  
249 experimental settings are presented in the supplementary Sect.S3. The experiment results indicate that when using the same  
250 emission inventory as the coarse-resolution simulation, the high-resolution simulation still show poor model performances in  
251 capturing the spatial variability of NO<sub>2</sub> concentrations in the PRD region, with calculated correlation coefficient only of 0.03  
252 and 0.02 for 15km and 5km resolutions, respectively ( supplementary Sect. S3, Fig. S5-6 and Table S3). Thus, the poor model  
253 performance in the PRD region could be more related to the coarse resolution and/or inappropriate spatial allocation of the  
254 emission inventories. These results also suggested that only increasing the resolutions of model may not help improve the  
255 model performance.

256 Figure 3 presents the monthly timeseries of the observed and simulated regional mean NO<sub>2</sub> concentrations over the NCP  
257 (3a) and PRD (3b) regions from January to December in 2010. The models well captured the monthly variations of NO<sub>2</sub>  
258 concentrations both in the NCP and PRD regions. According to Table 2, the correlation coefficient ranges from 0.28 to 0.96  
259 in the NCP region and from 0.52 to 0.95 in the PRD region. M8 showed the largest overestimation among all models in summer  
260 that MBE (NMB) can reach 12.1 ppbv (75.8%) in the NCP region, which may help explain the low correlation of this model.  
261 M9 exhibited a significant overestimation in winter in the NCP region with MBE (NMB) up to 22.0 ppbv (79.3%) while much  
262 less overestimation or even underestimation (summer) in other seasons. This discrepancy may be explained by that M9 was  
263 an online coupled model which considers two-way coupling effects between the meteorology and chemistry. During the period  
264 with heavy haze, the radiation can be largely reduced by aerosol dimming effects, leading to weakened photochemistry,  
265 lowered boundary layer height and thus the increase of NO<sub>2</sub> concentrations. Severe haze was reported to occur in North China  
266 in January 2010, with maximum hourly PM<sub>2.5</sub> concentration even reached as high as ~500 µg/m<sup>3</sup> in urban Beijing (Gao et al.,  
267 2018). Such high aerosol loadings in atmosphere could trigger interactions between chemistry and meteorology. Interestingly,  
268 M9 did not overestimate NO<sub>2</sub> during winter in the PRD region. This might be related to the lower aerosol concentrations and  
269 weaker chemistry-and-meteorology coupling effects in the PRD region.



### 270 3.1.2 CO

271 Similar analyses were performed for modeling results of CO. All models significantly underestimated the annual mean  
272 CO concentrations both in the NCP and PRD regions (Figs. 2c-d and Table 2). Calculated MBE (NMB) ranges from -1.69  
273 ppmv (-76.2%) to -1.16 ppmv (-52.0%) in the NCP region and from -0.67 ppmv (-69.6%) to -0.50 ppmv (-52.3%) in the PRD  
274 region (Table 2). Such large negative biases in all models were not likely to be explained by the model uncertainties, suggesting  
275 the negative biases in the CO emissions over China. This is consistent with the inversion results of Tang et al., 2013 which  
276 indicates a significant underestimation of CO emissions over the Beijing and surrounding areas in the summer of 2010. Over  
277 the latest decades, global models also reported CO underestimations in north hemisphere (Naik et al., 2013; Stein et al., 2014)  
278 and a number of global model inversion studies have been conducted to derive the optimized CO emissions. Most of these  
279 studies have reported a significant underestimation of CO emissions in their *a priori* estimates (Bergamaschi et al.,  
280 2000; Miyazaki et al., 2012; Petron et al., 2002; Petron et al., 2004). Our findings agree with these studies and indicate that more  
281 accurate CO emissions are needed in future studies. Model performances in simulating spatial variability of CO concentrations  
282 were still poor in the PRD region according to Table 2 with most models showing negative correlation coefficients.

283 Timeseries of the observed and simulated regional mean CO concentrations in the NCP and PRD regions are presented  
284 in Fig.3c-d. It shows that the models well reproduced the monthly variations of CO concentrations in both the NCP and PRD  
285 regions with high temporal correlation coefficient except M5 (Table 2). All models, however, underestimated CO  
286 concentrations throughout the year and showed largest underestimations in winter with MBE (NMB) by ensemble mean up to  
287 -2.1 ppmv (-64.9%) in the NCP region and -0.75 ppmv (-60.6%) in the PRD region.

### 288 3.1.3 NH<sub>3</sub>

289 Figure 2e shows the comparisons of the observed and simulated annual mean NH<sub>3</sub> concentrations in the NCP region.  
290 Since we used the NH<sub>3</sub> observations from September 2015 to August 2016, negative biases are expected according to the  
291 increasing trend of atmospheric ammonia during period 2003–2016 detected by recently retrievals from the Atmospheric  
292 Infrared Sounder (AIRS) aboard NASA's Aqua satellite (Warner et al., 2016; Warner et al., 2017). Due to the interannual  
293 uncertainty, we mainly focused on the disparities among different models rather than the deviation from observations.

294 Large differences can be seen in simulated NH<sub>3</sub> concentrations from different models. M14 simulated very low  
295 concentrations and exhibited the largest negative biases with MBE (NMB) of -12.2 ppbv (-66.3%), which may be related to  
296 the higher conversion rate of NH<sub>3</sub> to NH<sub>4</sub><sup>+</sup> in M14 (discussed in later part of this section). On the contrary, M9 provided much  
297 higher NH<sub>3</sub> concentrations than other models with MBE (NMB) up to 21.8 ppbv (118.7%). For the CMAQ models, M1 and  
298 M2 exhibited higher NH<sub>3</sub> concentrations and larger spatial variability compared to other CMAQ models. Such discrepancy  
299 may be explained by that M1 and M2 are two model runs using CMAQ v5.0.2. The bi-directional exchange of NH<sub>3</sub> has been  
300 integrated into CMAQ from version 5.0. This module can simulate the emitted and deposited processes of NH<sub>3</sub> between

301 atmosphere and the surfaces, allowing the additional NH<sub>3</sub> emissions to the atmosphere (US EPA Office of Research and  
302 Development).

303 As can be seen in Table 2, the observed spatial variations of NH<sub>3</sub> over the NCP region can be well reproduced by all  
304 models ( $R = 0.57-0.71$ ), indicating that the spatial variations of current NH<sub>3</sub> emissions over the NCP region are well represented  
305 in emission inventories. However, all models failed to capture the observed monthly variations of NH<sub>3</sub> concentrations with  
306 most models mismatching the observed NH<sub>3</sub> peak (July) and showing negative correlation coefficients. M10 and M13 are  
307 exceptions showing good temporal correlations of 0.64 and 0.65, respectively (Fig. 3e and Table 2). This is quite different  
308 from the model behavior in simulating the monthly variations of NO<sub>2</sub> and CO concentrations. As seen in Fig. 3e, the  
309 observation showed the peak concentrations of NH<sub>3</sub> in summer months and lower concentrations in autumn and winter, which  
310 is consistent with the previous NH<sub>3</sub> observations in the NCP region (Shen et al., 2011; Xu et al., 2016; Meng et al., 2011).  
311 Newly derived satellite-measured NH<sub>3</sub> at 918 hPa averaged between September 2002 and August 2015 also demonstrated  
312 higher concentrations in spring and summer and lower concentrations in autumn and winter (Warner et al., 2016). However,  
313 all models predicted a peak concentration in November except M10 in August in and M13 in June. We also used the satellite  
314 retrievals of NH<sub>3</sub> total columns from IASI to further evaluate the modeled monthly variations of NH<sub>3</sub> concentrations, since  
315 evaluating the model results using observations from different years may be inappropriate due to the emission change of NH<sub>3</sub>.  
316 Comparisons of the surface NH<sub>3</sub> observations from AMoN-China and NH<sub>3</sub> total columns from IASI (supplementary Fig.S7)  
317 suggest that the IASI measurement can well represent the monthly variations of surface NH<sub>3</sub> concentrations, which can be  
318 used to qualitatively evaluate the modeled monthly variations of surface NH<sub>3</sub> concentrations. The monthly time series of the  
319 regional mean NH<sub>3</sub> total columns over the NCP region from January, 2008 to December, 2016 are shown in supplementary  
320 Fig. S8, which shows similar monthly variations to the surface NH<sub>3</sub> observations with highest value in July and confirms the  
321 poor model performances in reproducing the monthly variations of NH<sub>3</sub> concentrations. The IASI measurement also indicates  
322 that the interannual variability of monthly variations of NH<sub>3</sub> concentrations over the NCP region was small from year 2008 to  
323 2016, which suggest that using observations from different years could still provide valuable clues for verifying the modeled  
324 monthly variations.

325 The simulated monthly variations of NH<sub>3</sub> concentrations were closely related to the monthly variations of the NH<sub>3</sub>  
326 emissions. Most models predicted three peak values of NH<sub>3</sub> concentrations in June, August and November but exhibited a  
327 significant decrease in July, which was in good agreement with the peaks and drops of the NH<sub>3</sub> emission rates in these months  
328 (Fig.4). The strong relationship between the simulated NH<sub>3</sub> concentrations and the emission rates suggests that the poor model  
329 performance in reproducing the monthly variations of NH<sub>3</sub> concentrations is probably related to the uncertainties in the monthly  
330 variations of NH<sub>3</sub> emissions. This is consistent with the recent bottom-up and top-down estimates of agriculture ammonia  
331 emissions in China by (Zhang et al., 2018), which shows more distinct seasonality of Chinese NH<sub>3</sub> emissions.

332 It is worth noting that there are also important uncertainties in the models beyond emission uncertainty. In order to  
333 investigate this issue, we have analyzed the impact of gas-aerosol partitioning of NH<sub>3</sub> on the simulations of NH<sub>3</sub> concentrations.  
334 Figure 5 shows the timeseries of the simulated total ammonium (NH<sub>x</sub> = NH<sub>3</sub> + NH<sub>4</sub><sup>+</sup>) in the atmosphere along with the ratio

335 of gaseous  $\text{NH}_3$  to the total ammonium. M10 is excluded in Fig.5 since the GOCART model does not predict  $\text{NH}_4^+$   
336 concentrations. As a result, the emitted  $\text{NH}_3$  would be only presented as the gas phase in M10, leading to higher  $\text{NH}_3$  predictions.  
337 This may also help explain the different monthly variations of  $\text{NH}_3$  concentrations seen in M10. Without the considerations of  
338  $\text{NH}_4^+$ , the monthly variations of  $\text{NH}_3$  concentrations in M10 were more consistent with the monthly variations of  $\text{NH}_3$   
339 emissions, which highlighted the importance of gas-aerosol partitioning of  $\text{NH}_3$  on the predictions of monthly variations of  
340  $\text{NH}_3$  concentrations. As seen in fig.5, there are large discrepancy in the simulated gas-aerosol partitioning of  $\text{NH}_3$  from different  
341 models. M7 and M9 showed higher  $\text{NH}_3/\text{NH}_x$  ratio than other models, which means that these two models tended to retain the  
342  $\text{NH}_3$  in the gas phase and thus predicted higher  $\text{NH}_3$  concentrations than other models. For example, M7 predicted comparable  
343 magnitude of total ammonium with most models, while gas  $\text{NH}_3$  concentration in M7 accounted for more than 60% of total  
344 ammonium in summer and even 90% in winter. The lower conversion rate of  $\text{NH}_3$  to  $\text{NH}_4^+$  in M9 may be related to the gas  
345 phase chemistry used in the model. M9 used the RADM2 mechanism which gives lower reaction rates of oxidation of  $\text{SO}_2$  and  
346  $\text{NO}_2$  by the OH radical as compiled by Tan et al., 2019, leading to lower productions of acid and thus lower conversion rate of  
347  $\text{NH}_3$  to  $\text{NH}_4^+$ . In case of M7, the hydrolysis of  $\text{N}_2\text{O}_5$  was not considered in M7, which leads to a lower tendency in the prediction  
348 of  $\text{NO}_3^-$  (Chen et al., 2019) and partly explains the higher  $\text{NH}_3$  predictions of M7. On the contrary, M14 showed a much lower  
349  $\text{NH}_3/\text{NH}_x$  ratio than most models, which would be related to its higher production rates of sulfate than other models as seen in  
350 Chen et al., 2019. In terms of monthly variations, most models predicted lower  $\text{NH}_3/\text{NH}_x$  ratio in summer than that in other  
351 seasons, suggesting the higher conversion rates of  $\text{NH}_3$  from gas phase to aerosol phase in summer. This would be related to  
352 the higher yield of ammonium sulfate due to the enhanced photochemical oxidation activity in summer. However, different  
353 from the modeling results, the  $\text{NH}_3$  and  $\text{NH}_4^+$  observations over the NCP region indicated a lower  $\text{NH}_3/\text{NH}_x$  ratio with higher  
354 ammonium concentrations in autumn and winter (Shen et al., 2011; Xu et al., 2016). Although observed  $\text{NH}_4^+$  was largest in  
355 summer at a rural site in Beijing, observed  $\text{NH}_3/\text{NH}_x$  ratio was still highest in summer according to observations from Meng  
356 et al., 2011. These results indicate that there would be large uncertainties in the modeling of seasonal variations of the gas-  
357 aerosol partitioning of  $\text{NH}_3$  over the NCP region. The formation of  $\text{NH}_4^+$  mainly depends on the acid gas concentrations,  
358 temperature, water availability (Khoder, 2002) and the flux rates of  $\text{NH}_3$  (Nemitz et al., 2001). Compared with spring and  
359 summer, the lower temperature and higher  $\text{SO}_2$  and  $\text{NO}_x$  emissions should favor the gas-to-particle phase conversion of  $\text{NH}_3$   
360 and lead to higher  $\text{NH}_4^+$  concentrations. This contrast indicates that some reaction pathways of acid productions ( $\text{H}_2\text{SO}_4$  or  
361  $\text{HNO}_3$ ) may be missing in current models, such as aqueous-phase and heterogeneous chemistry (Cheng et al., 2016; Wang et  
362 al., 2016; Zheng et al., 2015). Such uncertainty may be another important factor contributing to the poor model performances  
363 in reproducing the monthly variations of  $\text{NH}_3$  concentrations over the NCP region.

### 364 **3.2 Quantifying the impacts of model uncertainty**

365 In this section, we further investigate the discrepancies among the different models to quantify the impacts of model  
366 uncertainty on the simulations of these gases. As we mentioned in Sect. 2, most of these models employed common

367 meteorology fields and emission inventories over China under the same modeling domain and horizontal resolutions, which  
368 composed an appropriate set for investigating the model uncertainties.

369 Figures 6–8 present the simulated annual mean concentrations of NO<sub>2</sub>, CO and NH<sub>3</sub> from different models. The spatial  
370 distributions of the simulated NO<sub>2</sub>, CO and NH<sub>3</sub> concentrations from different models agreed well with each other, similar to  
371 the spatial distributions of their emissions (Fig. 1). High NO<sub>2</sub> concentrations were mainly located in the north and central-east  
372 China, and several hot-spots of NO<sub>2</sub> were also detected in the northeast China and the PRD region. M5, M8, M9, and M11  
373 predicted higher NO<sub>2</sub> concentrations than other models especially for M8 which also predicted very high NO<sub>2</sub> levels over  
374 southeast China. Similar to NO<sub>2</sub>, high CO concentrations were generally located over the north and central-east China as well  
375 as the east of Sichuan basin. M8, M9 and M11 predicted higher CO concentrations than other models as well. In terms of NH<sub>3</sub>,  
376 although most models shared similar spatial patterns of NH<sub>3</sub> simulations, the simulated NH<sub>3</sub> concentrations varied largely from  
377 different models. High NH<sub>3</sub> concentrations were mainly located over the north China and India peninsula, which was in  
378 accordance with the distribution of agricultural activity intensity over East Asia. Among these models, M9 and M10 produced  
379 much higher NH<sub>3</sub> concentrations over East Asia while M4, M5, M6, M13 and M14 produced much lower concentrations.

380 The impacts of model uncertainty on the simulations of NH<sub>3</sub> (9a), CO (9b) and NO<sub>2</sub> (9c) were then quantified in Fig.9,  
381 denoted by the spatial distributions of the standard deviation (ensemble spread) and the corresponding distributions of CV on  
382 the annual and seasonal basis. Note that M13 and M14 were excluded in the calculation of ensemble spread and CV to reduce  
383 the influences of the meteorological input data and horizontal resolutions. It seems that the impacts of model uncertainty  
384 increase with the reactivity of gases. NH<sub>3</sub> simulations were affected most by the model uncertainty, while CO suffered least  
385 from the uncertainty in models.

386 The ensemble spread of NH<sub>3</sub> simulations exhibited a strong spatial variability with higher values mainly located in the  
387 NCP region. Standard deviation of the annual mean NH<sub>3</sub> concentrations can be over 20 ppbv in Henan province and 15 ppbv  
388 in the south of Hebei province, which is about 60–80% and 40–60% of the ensemble mean respectively according to the CV  
389 distribution. As we mentioned in Sect. 3.1.3, these large modeling differences can be partly explained by the differences in the  
390 bi-directional exchange and gas-aerosol partitioning of NH<sub>3</sub> in different models. A strong seasonal pattern was also found in  
391 the differences of NH<sub>3</sub> simulations over the NCP region. The ensemble spread was smallest in spring while largest in autumn,  
392 up to 25 ppbv in most areas of the NCP region. However, in the relative sense, the modeling differences were larger in summer  
393 and winter while less in spring and autumn. The southeast China shared a similar magnitude of the ensemble spread (2–5 ppbv)  
394 and showed weaker seasonal variability. However, the modeling differences in the relative sense were larger than that in the  
395 NCP region with CV over 1.0 in all seasons except that in Summer. This can be due to that the simulated concentrations may  
396 be more influenced by the model processes over the areas with low emissions, while more constrained by the emissions over  
397 high emission rate areas.

398 CO was least affected by the model uncertainty among the three gases which is consistent with its weaker chemical  
399 activity and longer lifetime in the atmosphere. The ensemble spread of annual mean CO concentration was about 0.05–0.2  
400 ppmv in the east China, only about 20%–30% of the ensemble mean. Meanwhile, CO modeling differences was more

401 uniformly distributed in east China with CV less than 0.3 over most areas of east China. However, large modeling differences  
402 were visible over Myanmar during spring when there were high CO emissions from biomass burning. Model differences turned  
403 to be larger during winter in the NCP region with ensemble spread and CV about 0.3–0.5 ppmv and 0.3–0.4, respectively.

404 NO<sub>2</sub> was mediumly affected by the model uncertainty among the three gases. Ensemble spread of annual mean NO<sub>2</sub>  
405 concentration was 5–7.5 ppbv in the NCP region and 2.5–5 ppbv in the southeast China, which accounted for about 20%–30%  
406 of the ensemble mean in the former but more than 70% in the latter. The ensemble spread was largest in winter which was  
407 over 10 ppbv in the NCP region (30%–40%) and 5–7.5 ppbv in southeast China (over 70%). Similar to NH<sub>3</sub>, southeast China  
408 exhibited more modeling differences than the NCP region in relative sense with CV higher than 0.7 in most areas of southeast  
409 China.

#### 410 **4 Summary**

411 In this study, thirteen modeling results of surface NO<sub>2</sub>, CO and NH<sub>3</sub> concentrations from MICS-Asia III were compared  
412 with each other and evaluated against the observations over the NCP and PRD regions. Three questions are trying to be  
413 addressed which are related to the performance of current CTMs in simulating the NO<sub>2</sub>, CO and NH<sub>3</sub> concentrations over the  
414 highly industrialized regions of China, potential factors responsible for the model deviations from observations and differences  
415 among models, and the impacts of model uncertainty on the simulations of these gases.

416 Most models showed underestimations of NO<sub>2</sub> concentrations in the NCP and PRD regions, which could be an important  
417 potential factor contributing to the overpredicted O<sub>3</sub> concentrations in these regions. According to Xu et al., 2013, such  
418 underestimations would also be related to the positive biases in the NO<sub>2</sub> observations. The models showed better NO<sub>2</sub> model  
419 performance in the NCP region than that in the PRD region with smaller biases and RMSE. Most models well reproduced the  
420 observed temporal and spatial patterns of NO<sub>2</sub> concentrations in the NCP region, while relatively poor model performance was  
421 found in the PRD region in terms of the spatial variations of NO<sub>2</sub> concentrations. A sensitivity test with finer horizontal  
422 resolutions has been conducted to investigate the potential reasons for the poor model performance in the PRD region. The  
423 results shows that only increasing the model resolution cannot improve the model performance in the PRD region, which  
424 suggest that the poor model performance in the PRD region would be more related to the coarse resolution and/or inappropriate  
425 spatial allocations of the emission inventories in the PRD regions. All models significantly underestimated the CO  
426 concentrations in the NCP and PRD regions throughout the year. Such large underestimations of all models are not likely to  
427 be fully explained by the model uncertainty, which suggests that CO emissions may be underestimated in current emission  
428 inventories. More accurate estimate of CO emissions is thus needed for year 2010. Underestimations of CO emissions may be  
429 alleviated in recent years due to the decreasing trends of the Chinese CO emissions in recent years(Jiang et al., 2017;Zhong et  
430 al., 2017;Sun et al., 2018;Muller et al., 2018;Zheng et al., 2018;Zheng et al., 2019). The inversion results of Zheng et al., 2018  
431 also agree well with the MEIC inventory for CO emissions in China from 2013 to 2015. However uncertainties still exist in  
432 the CO emissions for recent years, according to previous studies, the estimated CO emissions in China ranges from 134–202

433 Tg/yr in year 2013 (Jiang et al., 2017;Zhong et al., 2017;Sun et al., 2018;Muller et al., 2018;Zheng et al., 2018;Zheng et al.,  
434 2019). Zhao et al., 2017 also suggested a -29%–40% uncertainty of CO emissions from the industrial sector in year 2012. For  
435 NH<sub>3</sub> simulations, in contrast to the good skills in the monthly variations of NO<sub>2</sub> and CO concentrations, all models failed to  
436 reproduce the observed monthly variations of NH<sub>3</sub> concentrations in the NCP region, as shown by both the surface and satellite  
437 measurements. Most models mismatched the observed peak and showed negative correlation coefficient with observations,  
438 which may be closely related to the uncertainty in the monthly variations of NH<sub>3</sub> emissions and also the uncertainty in the gas-  
439 aerosol partitioning of NH<sub>3</sub>.

440 Several potential factors were found to be responsible for the model deviation and differences, including the emission  
441 inventories, chemistry-and-meteorology coupling effects, bi-directional exchange of NH<sub>3</sub> and the NH<sub>3</sub> gas-aerosol partitioning,  
442 which would be important aspects with respect to the model improvements in future. Previous studies also suggest that the  
443 nitrous acid (HONO) chemistry plays an important role in the atmospheric nitrogen chemistry, which influences the  
444 simulations of NO<sub>2</sub> and NH<sub>3</sub> (Fu et al., 2019;Zhang et al., 2017;Zhang et al., 2016). Heterogeneous conversion from NO<sub>2</sub> to  
445 HONO ( $2\text{NO}_{2(g)} + \text{H}_2\text{O}_{(l)} \rightarrow \text{HONO}_{(l)} + \text{HNO}_{3(l)}$ ) is one of the dominant sources of HONO in the atmosphere, which has been  
446 considered in most models of MICS-Asia III, including CMAQ since version 4.7, NAQPMS, NHM-Chem and GEOS-Chem.  
447 However, some other important sources of HONO may still be underestimated by models in MICS-Asia III. For example, Fu  
448 et al., 2019 suggested that the high relative humidity and strong light could enhance the heterogeneous reaction of NO<sub>2</sub>, and  
449 the photolysis of total nitrate were also important sources of HONO. These sources has not been included in the models of  
450 MICS-Asia III, which would lead to the deviations from observations. The inter-comparisons of the ensemble models  
451 quantified the impacts of model uncertainty on the simulations of these gases, which shows that the impacts of model  
452 uncertainty increases with the reactivity of these gases. Models contained more uncertainties in the prediction of NH<sub>3</sub> than the  
453 other two gases. Based on these findings, some recommendations are made for future studies:

454 1) More accurate estimation of CO and NH<sub>3</sub> emissions are needed in future studies. Both bottom-up and top-down method  
455 (inversion technique) can help address this problem. The inversion of NH<sub>3</sub> emissions would be more complicated than the  
456 inversion of CO emissions due to the larger uncertainties in modeling the atmospheric processes of NH<sub>3</sub>. Nevertheless, it could  
457 still provide valuable clues for verifying the bottom-up emission inventories (Zhang et al., 2009) if the models were well  
458 validated. In addition, by using the ground or satellite measurements, the top-down methods could also give valuable  
459 information on the spatial and temporal patterns of NH<sub>3</sub> emissions, such as the inversions studies by Paulot et al., 2014 and  
460 Zhang et al., 2018. However, more attention should be paid to the validations of model before the inversion estimation of NH<sub>3</sub>  
461 emissions. How to represent the model uncertainties in the current framework of emission inversion is also an important aspect  
462 in future studies. Things could be better for CO considering its small and weakly spatial-dependent model uncertainties.

463 2) For some highly active and/or short-lived primary pollutants, like NH<sub>3</sub>, model uncertainty can also take a great part in  
464 the forecast uncertainty. Emission uncertainty alone may not be sufficient to explain the forecast uncertainty and may cause  
465 underdispersive, and overconfident forecasts. Future studies are needed in how to better represent the model uncertainties in

466 the model predictions to obtain a better forecast skill. Such model uncertainties also emphasize the need to validate the  
467 individual model before using its results to make important policy recommendation.

468 3) Gas-aerosol partition of  $\text{NH}_3$  is shown to be an important source of uncertainties in  $\text{NH}_3$  simulation. The formation of  
469  $\text{NH}_4^+$  particles is mainly limited by the availability of  $\text{H}_2\text{SO}_4$  and  $\text{HNO}_3$  under ammonia-rich conditions, which involves  
470 complex chemical reactions, including gas-phase, aqueous-phase and heterogeneous chemistry (Cheng et al., 2016; Wang et  
471 al., 2016; Zheng et al., 2015). These processes are needed to be verified and incorporated into models to better represent the  
472 chemistry in the atmosphere.

473 4) The gas chemistry mechanisms used in this study are SAPRC 99, CB05, CBMZ, RACM and RADM2, and some of  
474 them have an updated version such as CB06 and SPARC 07. Our conclusions may not be applicable to these newer versions  
475 of mechanisms and thus more comparisons studies can be performed to understand the differences in these new mechanisms.

#### 476 **Competing interests**

477 The authors declare that they have no conflict of interest.

#### 478 **Author contribution**

479 X.T., J.Z., Z.F.W and G.C. conducted the design of this study. J.F., X.W., S.I., K.Y., T.N., H.L., C.K., C.L., L.C., M.Z., Z.T.,  
480 J.L., M.K., H.L., B.G. contributed to the modelling data. Z.W. performed the simulations of standard meteorological field.  
481 M.L. and Q.W. provided the emission data. K.S. provided the CHASER output for boundary conditions. Y.W., Y.P., G.T.  
482 provided the observation data. L.K. and X.T. performed the analysis and prepared the manuscript with contributions from all-  
483 authors.

#### 484 **Acknowledgements**

485 This study was supported by the National Natural Science Foundation (Grant Nos. 91644216 & 41620104008), the National  
486 Key R&D Program (Grant Nos. 2018YFC0213503) and Guangdong Provincial Science and Technology Development Special  
487 Fund (No.2017B020216007). Yuepeng Pan acknowledges the National Key Research and Development Program of China  
488 (Grants 2017YFC0210100, 2016YFC0201802) and the National Natural Science Foundation of China (Grant 41405144) for  
489 financial support. We are indebted to the staff who collected the samples at the AMoN-China sites during the study period.

490 **References**

- 491 Anenberg, S. C., Horowitz, L. W., Tong, D. Q., and West, J. J.: An Estimate of the Global Burden of Anthropogenic Ozone  
492 and Fine Particulate Matter on Premature Human Mortality Using Atmospheric Modeling, *Environ. Health Perspect.*,  
493 118, 1189-1195, 10.1289/ehp.0901220, 2010.
- 494 Bergamaschi, P., Hein, R., Heimann, M., and Crutzen, P. J.: Inverse modeling of the global CO cycle 1. Inversion of CO  
495 mixing ratios, *J. Geophys. Res.-Atmos.*, 105, 1909-1927, 10.1029/1999jd900818, 2000.
- 496 Byun, D., and Schere, K. L.: Review of the governing equations, computational algorithms, and other components of the  
497 models-3 Community Multiscale Air Quality (CMAQ) modeling system, *Appl. Mech. Rev.*, 59, 51-77,  
498 10.1115/1.2128636, 2006.
- 499 Carmichael, G., Sakurai, T., Streets, D., Hozumi, Y., Ueda, H., Park, S., Fung, C., Han, Z., Kajino, M., and Engardt, M.:  
500 MICS-Asia II: The model intercomparison study for Asia Phase II methodology and overview of findings, *Atmos.*  
501 *Environ.*, 42, 3468-3490, 10.1016/j.atmosenv.2007.04.007, 2008.
- 502 Carmichael, G. R., Calori, G., Hayami, H., Uno, I., Cho, S. Y., Engardt, M., Kim, S. B., Ichikawa, Y., Ikeda, Y., Woo, J. H.,  
503 Ueda, H., and Amann, M.: The MICS-Asia study: model intercomparison of long-range transport and sulfur deposition  
504 in East Asia, *Atmos. Environ.*, 36, 175-199, 10.1016/s1352-2310(01)00448-4, 2002.
- 505 Chen, L., Gao, Y., Zhang, M., Fu, J. S., Zhu, J., Liao, H., Li, J., Huang, K., Ge, B., Wang, X., Lam, Y. F., Lin, C. Y., Itahashi,  
506 S., Nagashima, T., Kajino, M., Yamaji, K., Wang, Z., and Kurokawa, J. I.: MICS-Asia III: Multi-model comparison and  
507 evaluation of aerosol over East Asia, *Atmos. Chem. Phys. Discuss.*, 2019, 1-54, 10.5194/acp-2018-1346, 2019.
- 508 Cheng, Y. F., Zheng, G. J., Wei, C., Mu, Q., Zheng, B., Wang, Z. B., Gao, M., Zhang, Q., He, K. B., Carmichael, G., Poschl,  
509 U., and Su, H.: Reactive nitrogen chemistry in aerosol water as a source of sulfate during haze events in China, *Sci. Adv.*,  
510 2, 11, 10.1126/sciadv.1601530, 2016.
- 511 Dabberdt, W. F., and Miller, E.: Uncertainty, ensembles and air quality dispersion modeling: applications and challenges,  
512 *Atmos. Environ.*, 34, 4667-4673, 10.1016/s1352-2310(00)00141-2, 2000.
- 513 Dentener, F. J., and Crutzen, P. J.: REACTION OF N2O5 ON TROPOSPHERIC AEROSOLS - IMPACT ON THE GLOBAL  
514 DISTRIBUTIONS OF NOX, O3, AND OH, *J. Geophys. Res.-Atmos.*, 98, 7149-7163, 10.1029/92jd02979, 1993.
- 515 Evans, M. J., and Jacob, D. J.: Impact of new laboratory studies of N2O5 hydrolysis on global model budgets of tropospheric  
516 nitrogen oxides, ozone, and OH, *Geophys. Res. Lett.*, 32, 4, 10.1029/2005gl022469, 2005.
- 517 Fine, J., Vuilleumier, L., Reynolds, S., Roth, P., and Brown, N.: Evaluating uncertainties in regional photochemical air quality  
518 modeling, *Annu. Rev. Environ. Resour.*, 28, 59-106, 10.1146/annurev.energy.28.011503.163508, 2003.
- 519 Fu, X., Wang, T., Zhang, L., Li, Q. Y., Wang, Z., Xia, M., Yun, H., Wang, W. H., Yu, C., Yue, D. L., Zhou, Y., Zheng, J. Y.,  
520 and Han, R.: The significant contribution of HONO to secondary pollutants during a severe winter pollution event in  
521 southern China, *Atmos. Chem. Phys.*, 19, 1-14, 10.5194/acp-19-1-2019, 2019.



522 Galmarini, S., Bianconi, R., Klug, W., Mikkelsen, T., Addis, R., Andronopoulos, S., Astrup, P., Baklanov, A., Bartniki, J.,  
523 Bartzis, J. C., Bellasio, R., Bompay, F., Buckley, R., Bouzom, M., Champion, H., D'Amours, R., Davakis, E., Eleveld,  
524 H., Geertsema, G. T., Glaab, H., Kollax, M., Ilvonen, M., Manning, A., Pechinger, U., Persson, C., Polreich, E., Potemski,  
525 S., Prodanova, M., Saltbones, J., Slaper, H., Sofiev, M. A., Syrakov, D., Sørensen, J. H., Auwera, L. V. d., Valkama, I.,  
526 and Zelazny, R.: Ensemble dispersion forecasting—Part I: concept, approach and indicators, *Atmos. Environ.*, 38, 4607-  
527 4617, <https://doi.org/10.1016/j.atmosenv.2004.05.030>, 2004.

528 Gao, D. F., Stockwell, W. R., and Milford, J. B.: Global uncertainty analysis of a regional-scale gas-phase chemical mechanism,  
529 *J. Geophys. Res.-Atmos.*, 101, 9107-9119, 10.1029/96jd00060, 1996.

530 Gao, M., Han, Z. W., Liu, Z. R., Li, M., Xin, J. Y., Tao, Z. N., Li, J. W., Kang, J. E., Huang, K., Dong, X. Y., Zhuang, B. L.,  
531 Li, S., Ge, B. Z., Wu, Q. Z., Cheng, Y. F., Wang, Y. S., Lee, H. J., Kim, C. H., Fu, J. S. S., Wang, T. J., Chin, M. A.,  
532 Woo, J. H., Zhang, Q., Wang, Z. F., and Carmichael, G. R.: Air quality and climate change, Topic 3 of the Model Inter-  
533 Comparison Study for Asia Phase III (MICS-Asia III) - Part 1: Overview and model evaluation, *Atmos. Chem. Phys.*, 18,  
534 4859-4884, 10.5194/acp-18-4859-2018, 2018.

535 Gillenwater, M.: Forgotten carbon: indirect CO<sub>2</sub> in greenhouse gas emission inventories, *Environ. Sci. Policy*, 11, 195-203,  
536 10.1016/j.envsci.2007.09.001, 2008.

537 Grell, G. A., Peckham, S. E., Schmitz, R., McKeen, S. A., Frost, G., Skamarock, W. C., and Eder, B.: Fully coupled "online"  
538 chemistry within the WRF model, *Atmos. Environ.*, 39, 6957-6975, 10.1016/j.atmosenv.2005.04.027, 2005.

539 Guenther, A., Karl, T., Harley, P., Wiedinmyer, C., Palmer, P. I., and Geron, C.: Estimates of global terrestrial isoprene  
540 emissions using MEGAN (Model of Emissions of Gases and Aerosols from Nature), *Atmos. Chem. Phys.*, 6, 3181-3210,  
541 2006.

542 Han, K. M., Song, C. H., Ahn, H. J., Park, R. S., Woo, J. H., Lee, C. K., Richter, A., Burrows, J. P., Kim, J. Y., and Hong, J.  
543 H.: Investigation of NO<sub>x</sub> emissions and NO<sub>x</sub>-related chemistry in East Asia using CMAQ-predicted and GOME-derived  
544 NO<sub>2</sub> columns, *Atmos. Chem. Phys.*, 9, 17297-17341, 2008a.

545 Han, Z., Sakurai, T., Ueda, H., Carmichael, G., Streets, D., Hayami, H., Wang, Z., Holloway, T., Engardt, M., and Hozumi,  
546 Y.: MICS-Asia II: Model intercomparison and evaluation of ozone and relevant species, *Atmos. Environ.*, 42, 3491-3509,  
547 10.1016/j.atmosenv.2007.07.031, 2008b.

548 Janssens-Maenhout, G., Crippa, M., Guizzardi, D., Dentener, F., Muntean, M., Pouliot, G., Keating, T., Zhang, Q., Kurokawa,  
549 J., Wankmuller, R., van der Gon, H. D., Kuenen, J. J. P., Klimont, Z., Frost, G., Darras, S., Koffi, B., and Li, M.:  
550 HTAP\_v2.2: a mosaic of regional and global emission grid maps for 2008 and 2010 to study hemispheric transport of air  
551 pollution, *Atmos. Chem. Phys.*, 15, 11411-11432, 10.5194/acp-15-11411-2015, 2015.

552 Ji, D. S., Wang, Y. S., Wang, L. L., Chen, L. F., Hu, B., Tang, G. Q., Xin, J. Y., Song, T., Wen, T. X., Sun, Y., Pan, Y. P., and  
553 Liu, Z. R.: Analysis of heavy pollution episodes in selected cities of northern China, *Atmos. Environ.*, 50, 338-348,  
554 10.1016/j.atmosenv.2011.11.053, 2012.

555 Jiang, Z., Worden, J. R., Worden, H., Deeter, M., Jones, D. B. A., Arellano, A. F., and Henze, D. K.: A 15-year record of CO  
556 emissions constrained by MOPITT CO observations, *Atmos. Chem. Phys.*, 17, 4565-4583, 10.5194/acp-17-4565-2017,  
557 2017.

558 Jin, X. M., and Holloway, T.: Spatial and temporal variability of ozone sensitivity over China observed from the Ozone  
559 Monitoring Instrument, *J. Geophys. Res.-Atmos.*, 120, 7229-7246, 10.1002/2015jd023250, 2015.

560 Kajino, M., Inomata, Y., Sato, K., Ueda, H., Han, Z., An, J., Katata, G., Deushi, M., Maki, T., Oshima, N., Kurokawa, J.,  
561 Ohara, T., Takami, A., and Hatakeyama, S.: Development of the RAQM2 aerosol chemical transport model and  
562 predictions of the Northeast Asian aerosol mass, size, chemistry, and mixing type, *Atmos. Chem. Phys.*, 12, 11833-11856,  
563 10.5194/acp-12-11833-2012, 2012.

564 Kajino, M., Deushi, M., Sekiyama, T. T., Oshima, N., Yumimoto, K., Tanaka, T. Y., Ching, J., Hashimoto, A., Yamamoto, T.,  
565 Ikegami, M., Kamada, A., Miyashita, M., Inomata, Y., Shima, S. I., Adachi, K., Zaizen, Y., Igarashi, Y., Ueda, H., Maki,  
566 T., and Mikami, M.: NHM-Chem, the Japan Meteorological Agency's regional meteorology – chemistry model (v1.0):  
567 model description and aerosol representations, *Geosci. Model Dev. Discuss.*, 2018, 1-45, 10.5194/gmd-2018-128, 2018.

568 Khoder, M. I.: Atmospheric conversion of sulfur dioxide to particulate sulfate and nitrogen dioxide to particulate nitrate and  
569 gaseous nitric acid in an urban area, *Chemosphere*, 49, 675-684, 10.1016/s0045-6535(02)00391-0, 2002.

570 Kurokawa, J., Ohara, T., Morikawa, T., Hanayama, S., Janssens-Maenhout, G., Fukui, T., Kawashima, K., and Akimoto, H.:  
571 Emissions of air pollutants and greenhouse gases over Asian regions during 2000-2008: Regional Emission inventory in  
572 ASia (REAS) version 2, *Atmos. Chem. Phys.*, 13, 11019-11058, 10.5194/acp-13-11019-2013, 2013.

573 Lelieveld, J., Evans, J. S., Fnais, M., Giannadaki, D., and Pozzer, A.: The contribution of outdoor air pollution sources to  
574 premature mortality on a global scale, *Nature*, 525, 367-+, 10.1038/nature15371, 2015.

575 Levy, H.: NORMAL ATMOSPHERE - LARGE RADICAL AND FORMALDEHYDE CONCENTRATIONS PREDICTED,  
576 *Science*, 173, 141-&, 10.1126/science.173.3992.141, 1971.

577 Li, J., Du, H. Y., Wang, Z. F., Sun, Y. L., Yang, W. Y., Li, J. J., Tang, X., and Fu, P. Q.: Rapid formation of a severe regional  
578 winter haze episode over a mega-city cluster on the North China Plain, *Environ. Pollut.*, 223, 605-615,  
579 10.1016/j.envpol.2017.01.063, 2017a.

580 Li, J., Nagashima, T., Kong, L., Ge, B., Yamaji, K., Fu, J. S., Wang, X., Fan, Q., Itahashi, S., Lee, H. J., Kim, C. H., Lin, C.  
581 Y., Zhang, M., Tao, Z., Kajino, M., Liao, H., Li, M., Woo, J. H., Kurokawa, J. I., Wu, Q., Akimoto, H., Carmichael, G.  
582 R., and Wang, Z.: Model evaluation and inter-comparison of surface-level ozone and relevant species in East Asia in the  
583 context of MICS-Asia phase III Part I: overview, *Atmos. Chem. Phys. Discuss.*, 2019, 1-56, 10.5194/acp-2018-1283,  
584 2019.

585 Li, M., Zhang, Q., Kurokawa, J. I., Woo, J. H., He, K., Lu, Z., Ohara, T., Song, Y., Streets, D. G., Carmichael, G. R., Cheng,  
586 Y., Hong, C., Huo, H., Jiang, X., Kang, S., Liu, F., Su, H., and Zheng, B.: MIX: a mosaic Asian anthropogenic emission  
587 inventory under the international collaboration framework of the MICS-Asia and HTAP, *Atmos. Chem. Phys.*, 17, 935-  
588 963, 10.5194/acp-17-935-2017, 2017b.

589 Lu, M. M., Tang, X., Wang, Z. F., Gbaguidi, A., Liang, S. W., Hu, K., Wu, L., Wu, H. J., Huang, Z., and Shen, L. J.: Source  
590 tagging modeling study of heavy haze episodes under complex regional transport processes over Wuhan megacity,  
591 Central China, *Environ. Pollut.*, 231, 612-621, 10.1016/j.envpol.2017.08.046, 2017.

592 Ma, C. Q., Wang, T. J., Mizzi, A. P., Anderson, J. L., Zhuang, B. L., Xie, M., and Wu, R. S.: Multiconstituent Data Assimilation  
593 With WRF-Chem/DART: Potential for Adjusting Anthropogenic Emissions and Improving Air Quality Forecasts Over  
594 Eastern China, *J. Geophys. Res.-Atmos.*, 124, 7393-7412, 10.1029/2019jd030421, 2019.

595 Mallet, V., and Sportisse, B.: Uncertainty in a chemistry-transport model due to physical parameterizations and numerical  
596 approximations: An ensemble approach applied to ozone modeling, *J. Geophys. Res.-Atmos.*, 111, 15,  
597 10.1029/2005jd006149, 2006.

598 Meng, Z. Y., Lin, W. L., Jiang, X. M., Yan, P., Wang, Y., Zhang, Y. M., Jia, X. F., and Yu, X. L.: Characteristics of atmospheric  
599 ammonia over Beijing, China, *Atmos. Chem. Phys.*, 11, 6139-6151, 10.5194/acp-11-6139-2011, 2011.

600 Miyazaki, K., Eskes, H. J., Sudo, K., Takigawa, M., Weele, M. V., and Boersma, K. F.: Simultaneous assimilation of satellite  
601 NO<sub>2</sub>, O<sub>3</sub>, CO, and HNO<sub>3</sub> data for the analysis of tropospheric chemical composition and emissions, *Atmos. Chem. Phys.*  
602 & Discussions, 264, 1017-1023, 2012.

603 Muller, J. F., Stavrakou, T., Bauwens, M., George, M., Hurtmans, D., Coheur, P. F., Clerbaux, C., and Sweeney, C.: Top-  
604 Down CO Emissions Based On IASI Observations and Hemispheric Constraints on OH Levels, *Geophys. Res. Lett.*, 45,  
605 1621-1629, 10.1002/2017gl076697, 2018.

606 Naik, V., Voulgarakis, A., Fiore, A. M., Horowitz, L. W., Lamarque, J. F., Lin, M., Prather, M. J., Young, P. J., Bergmann,  
607 D., Cameron-Smith, P. J., Cionni, I., Collins, W. J., Dalsoren, S. B., Doherty, R., Eyring, V., Faluvegi, G., Folberth, G.  
608 A., Josse, B., Lee, Y. H., MacKenzie, I. A., Nagashima, T., van Noije, T. P. C., Plummer, D. A., Righi, M., Rumbold, S.  
609 T., Skeie, R., Shindell, D. T., Stevenson, D. S., Strode, S., Sudo, K., Szopa, S., and Zeng, G.: Preindustrial to present-  
610 day changes in tropospheric hydroxyl radical and methane lifetime from the Atmospheric Chemistry and Climate Model  
611 Intercomparison Project (ACCMIP), *Atmos. Chem. Phys.*, 13, 5277-5298, 10.5194/acp-13-5277-2013, 2013.

612 Nemitz, E., Milford, C., and Sutton, M. A.: A two-layer canopy compensation point model for describing bi-directional  
613 biosphere-atmosphere exchange of ammonia, *Q. J. R. Meteorol. Soc.*, 127, 815-833, 10.1256/smsqj.57305, 2001.

614 Noije, T. P. C. V., Eskes, H. J., Dentener, F. J., Stevenson, D. S., Ellingsen, K., Schultz, M. G., Wild, O., Amann, M., Atherton,  
615 C. S., and Bergmann, D. J.: Multi-model ensemble simulations of tropospheric NO<sub>2</sub> compared with GOME retrievals for  
616 the year 2000, *Atmos. Chem. Phys.*, 6, 2943-2979, 2006.

617 Novelli, P. C., Masarie, K. A., and Lang, P. M.: Distributions and recent changes of carbon monoxide in the lower troposphere,  
618 *J. Geophys. Res.-Atmos.*, 103, 19015-19033, 10.1029/98jd01366, 1998.

619 Pan, Y., Tian, S., Zhao, Y., Zhang, L., Zhu, X., Gao, J., Huang, W., Zhou, Y., Song, Y., Zhang, Q., and Wang, Y.: Identifying  
620 ammonia hotspots in China using a national observation network, *Environ. Sci. Technol.*, 52, 3926-3934,  
621 10.1021/acs.est.7b05235, 2018.

622 Pan, Y. P., Wang, Y. S., Tang, G. Q., and Wu, D.: Wet and dry deposition of atmospheric nitrogen at ten sites in Northern  
623 China, *Atmos. Chem. Phys.*, 12, 6515-6535, 10.5194/acp-12-6515-2012, 2012.

624 Paulot, F., Jacob, D. J., Pinder, R. W., Bash, J. O., Travis, K., and Henze, D. K.: Ammonia emissions in the United States,  
625 European Union, and China derived by high-resolution inversion of ammonium wet deposition data: Interpretation with  
626 a new agricultural emissions inventory (MASAGE\_NH3), *J. Geophys. Res.-Atmos.*, 119, 4343-4364,  
627 10.1002/2013jd021130, 2014.

628 Peters-Lidard, C. D., Kemp, E. M., Matsui, T., Santanello, J. A., Kumar, S. V., Jacob, J. P., Clune, T., Tao, W. K., Chin, M.,  
629 Hou, A., Case, J. L., Kim, D., Kim, K. M., Lau, W., Liu, Y. Q., Shi, J., Starr, D., Tan, Q., Tao, Z. N., Zaitchik, B. F.,  
630 Zavadsky, B., Zhang, S. Q., and Zupanski, M.: Integrated modeling of aerosol, cloud, precipitation and land processes at  
631 satellite-resolved scales, *Environ. Modell. Softw.*, 67, 149-159, 10.1016/j.envsoft.2015.01.007, 2015.

632 Petron, G., Granier, C., Khattatov, B., Lamarque, J. F., Yudin, V., Muller, J. F., and Gille, J.: Inverse modeling of carbon  
633 monoxide surface emissions using Climate Monitoring and Diagnostics Laboratory network observations, *J. Geophys.*  
634 *Res.-Atmos.*, 107, 23, 10.1029/2001jd001305, 2002.

635 Petron, G., Granier, C., Khattatov, B., Yudin, V., Lamarque, J. F., Emmons, L., Gille, J., and Edwards, D. P.: Monthly CO  
636 surface sources inventory based on the 2000-2001 MOPITT satellite data, *Geophys. Res. Lett.*, 31, 5,  
637 10.1029/2004gl020560, 2004.

638 Pielke, R. A., Cotton, W. R., Walko, R. L., Tremback, C. J., Lyons, W. A., Grasso, L. D., Nicholls, M. E., Moran, M. D.,  
639 Wesley, D. A., Lee, T. J., and Copeland, J. H.: A COMPREHENSIVE METEOROLOGICAL MODELING SYSTEM -  
640 RAMS, *Meteorol. Atmos. Phys.*, 49, 69-91, 10.1007/bf01025401, 1992.

641 Pinder, R. W., Adams, P. J., Pandis, S. N., and Gilliland, A. B.: Temporally resolved ammonia emission inventories: Current  
642 estimates, evaluation tools, and measurement needs, *J. Geophys. Res.-Atmos.*, 111, 14, 10.1029/2005jd006603, 2006.

643 Randerson, J. T., Werf, G. R. v. d., Giglio, L., Collatz, G. J., and Kasibhatla, P. S.: Global Fire Emissions Database, Version  
644 3 (GFEDv3.1). Data set. Available on-line [<http://daac.ornl.gov/>] from Oak Ridge National Laboratory Distributed Active  
645 Archive Center, Oak Ridge, Tennessee, USA. doi:10.3334/ORNLDAAAC/1191, 2013.

646 Rao, S. T., Galmarini, S., and Puckett, K.: Air Quality Model Evaluation International Initiative (AQMEII) Advancing the  
647 State of the Science in Regional Photochemical Modeling and Its Applications, *Bull. Amer. Meteorol. Soc.*, 92, 23-30,  
648 10.1175/2010bams3069.1, 2011.

649 Saito, K., Fujita, T., Yamada, Y., Ishida, J. I., Kumagai, Y., Aranami, K., Ohmori, S., Nagasawa, R., Kumagai, S., Muroi, C.,  
650 Kato, T., Eito, H., and Yamazaki, Y.: The operational JMA nonhydrostatic mesoscale model, *Mon. Weather Rev.*, 134,  
651 1266-1298, 10.1175/mwr3120.1, 2006.

652 Shao, M., Zhang, Y. H., Zeng, L. M., Tang, X. Y., Zhang, J., Zhong, L. J., and Wang, B. G.: Ground-level ozone in the Pearl  
653 River Delta and the roles of VOC and NO<sub>x</sub> in its production, *J. Environ. Manage.*, 90, 512-518,  
654 10.1016/j.jenvman.2007.12.008, 2009.

655 Shen, J. L., Liu, X. J., Zhang, Y., Fangmeier, A., Goulding, K., and Zhang, F. S.: Atmospheric ammonia and particulate  
656 ammonium from agricultural sources in the North China Plain, *Atmos. Environ.*, 45, 5033-5041,  
657 10.1016/j.atmosenv.2011.02.031, 2011.

658 Sillman, S.: The relation between ozone, NO<sub>x</sub> and hydrocarbons in urban and polluted rural environments, *Atmos. Environ.*,  
659 33, 1821-1845, 10.1016/s1352-2310(98)00345-8, 1999.

660 Skamarock, W. C.: A description of the advanced research WRF version 3, *Near Technical*, 113, 7-25, 2008.

661 Stein, O., Schultz, M. G., Bouarar, I., Clark, H., Huijnen, V., Gaudel, A., George, M., and Clerbaux, C.: On the wintertime  
662 low bias of Northern Hemisphere carbon monoxide found in global model simulations, *Atmos. Chem. Phys.*, 14, 9295-  
663 9316, 10.5194/acp-14-9295-2014, 2014.

664 Steinfeld, J. I.: *Atmos. Chem. Phys.: From Air Pollution to Climate Change*, Wiley, 1595-1595 pp., 1998.

665 Sun, W., Shao, M., Granier, C., Liu, Y., Ye, C. S., and Zheng, J. Y.: Long-Term Trends of Anthropogenic SO<sub>2</sub>, NO<sub>x</sub>, CO,  
666 and NMVOCs Emissions in China, *Earth Future*, 6, 1112-1133, 10.1029/2018ef000822, 2018.

667 Sun, Y. L., Wang, Z. F., Dong, H. B., Yang, T., Li, J., Pan, X. L., Chen, P., and Jayne, J. T.: Characterization of summer  
668 organic and inorganic aerosols in Beijing, China with an Aerosol Chemical Speciation Monitor, *Atmos. Environ.*, 51,  
669 250-259, 10.1016/j.atmosenv.2012.01.013, 2012.

670 Sun, Y. L., Wang, Z. F., Fu, P. Q., Yang, T., Jiang, Q., Dong, H. B., Li, J., and Jia, J. J.: Aerosol composition, sources and  
671 processes during wintertime in Beijing, China, *Atmos. Chem. Phys.*, 13, 4577-4592, 10.5194/acp-13-4577-2013, 2013.

672 Tan, J., Fu, J. S., Carmichael, G. R., Itahashi, S., Tao, Z., Huang, K., Dong, X., Yamaji, K., Nagashima, T., Wang, X., Liu, Y.,  
673 Lee, H. J., Lin, C. Y., Ge, B., Kajino, M., Zhu, J., Zhang, M., Hong, L., and Wang, Z.: Why models perform differently  
674 on particulate matter over East Asia? – A multi-model intercomparison study for MICS-Asia III, *Atmos. Chem. Phys.*  
675 *Discuss.*, 2019, 1-36, 10.5194/acp-2019-392, 2019.

676 Tang, G., Wang, Y., Li, X., Ji, D., Hsu, S., and Gao, X.: Spatial-temporal variations in surface ozone in Northern China as  
677 observed during 2009-2010 and possible implications for future air quality control strategies, *Atmos. Chem. Phys.*, 12,  
678 2757-2776, 10.5194/acp-12-2757-2012, 2012.

679 Tang, X., Zhu, J., Wang, Z. F., and Gbaguidi, A.: Improvement of ozone forecast over Beijing based on ensemble Kalman  
680 filter with simultaneous adjustment of initial conditions and emissions, *Atmos. Chem. Phys.*, 11, 12901-12916,  
681 10.5194/acp-11-12901-2011, 2011.

682 Tang, X., Zhu, J., Wang, Z. F., Wang, M., Gbaguidi, A., Li, J., Shao, M., Tang, G. Q., and Ji, D. S.: Inversion of CO emissions  
683 over Beijing and its surrounding areas with ensemble Kalman filter, *Atmos. Environ.*, 81, 676-686,  
684 10.1016/j.atmosenv.2013.08.051, 2013.

685 Uno, I., He, Y., Ohara, T., Yamaji, K., Kurokawa, J. I., Katayama, M., Wang, Z., Noguchi, K., Hayashida, S., Richter, A., and  
686 Burrows, J. P.: Systematic analysis of interannual and seasonal variations of model-simulated tropospheric NO<sub>2</sub> in Asia  
687 and comparison with GOME-satellite data, *Atmos. Chem. Phys.*, 7, 1671-1681, 10.5194/acp-7-1671-2007, 2007.

688 US EPA Office of Research and Development: CMAQv5.0, , doi:10.5281/zenodo.1079888, 2012.

689 Van Damme, M., Whitburn, S., Clarisse, L., Clerbaux, C., Hurtmans, D., and Coheur, P. F.: Version 2 of the IASI NH<sub>3</sub> neural  
690 network retrieval algorithm: near-real-time and reanalysed datasets, *Atmos. Meas. Tech.*, 10, 4905-4914, 10.5194/amt-  
691 10-4905-2017, 2017.

692 Van Damme, M., Clarisse, L., Whitburn, S., Hadji-Lazaro, J., Hurtmans, D., Clerbaux, C., and Coheur, P.-F.: Level 2 dataset  
693 and Level 3 oversampled average map of the IASI/Metop-A ammonia (NH<sub>3</sub>) morning column measurements (ANNI-  
694 NH<sub>3</sub>-v2.1R-I) from 2008 to 2016. PANGAEA, 2018.

695 von Bobruzki, K., Braban, C. F., Famulari, D., Jones, S. K., Blackall, T., Smith, T. E. L., Blom, M., Coe, H., Gallagher, M.,  
696 Ghalaieny, M., McGillen, M. R., Percival, C. J., Whitehead, J. D., Ellis, R., Murphy, J., Mohacsi, A., Pogany, A.,  
697 Junninen, H., Rantanen, S., Sutton, M. A., and Nemitz, E.: Field inter-comparison of eleven atmospheric ammonia  
698 measurement techniques, *Atmos. Meas. Tech.*, 3, 91-112, 10.5194/amt-3-91-2010, 2010.

699 Wang, G., Zhang, R., Gomez, M. E., Yang, L., Zamora, M. L., Hu, M., Lin, Y., Peng, J., Guo, S., and Meng, J.: Persistent  
700 sulfate formation from London Fog to Chinese haze, *Proc. Natl. Acad. Sci. U. S. A. of America*, 113, 13630, 2016.

701 Wang, Z. F., Maeda, T., Hayashi, M., Hsiao, L. F., and Liu, K. Y.: A nested air quality prediction modeling system for urban  
702 and regional scales: Application for high-ozone episode in Taiwan, *Water Air Soil Pollut.*, 130, 391-396,  
703 10.1023/a:1013833217916, 2001.

704 Warner, J. X., Wei, Z., Strow, L. L., Dickerson, R. R., and Nowak, J. B.: The global tropospheric ammonia distribution as seen  
705 in the 13-year AIRS measurement record, *Atmos. Chem. Phys.*, 16, 5467-5479, 10.5194/acp-16-5467-2016, 2016.

706 Warner, J. X., Dickerson, R. R., Wei, Z., Strow, L. L., Wang, Y., and Liang, Q.: Increased atmospheric ammonia over the  
707 world's major agricultural areas detected from space, *Geophys. Res. Lett.*, 44, 2875-2884, 10.1002/2016gl072305, 2017.

708 Xu, W., Wu, Q. H., Liu, X. J., Tang, A. H., Dore, A., and Heal, M.: Characteristics of ammonia, acid gases, and PM<sub>2.5</sub> for  
709 three typical land-use types in the North China Plain, *Environ. Sci. Pollut. Res.*, 23, 1158-1172, 10.1007/s11356-015-  
710 5648-3, 2016.

711 Xu, Z., Wang, T., Xue, L. K., Louie, P. K. K., Luk, C. W. Y., Gao, J., Wang, S. L., Chai, F. H., and Wang, W. X.: Evaluating  
712 the uncertainties of thermal catalytic conversion in measuring atmospheric nitrogen dioxide at four differently polluted  
713 sites in China, *Atmos. Environ.*, 76, 221-226, 10.1016/j.atmosenv.2012.09.043, 2013.

714 Xu, Z., Liu, M., Zhang, M., Song, Y., Wang, S., Zhang, L., Xu, T., Wang, T., Yan, C., Zhou, T., Sun, Y., Pan, Y., Hu, M.,  
715 Zheng, M., and Zhu, T.: High efficiency of livestock ammonia emission controls in alleviating particulate nitrate during  
716 a severe winter haze episode in northern China, *Atmos. Chem. Phys.*, 19, 5605-5613, 10.5194/acp-19-5605-2019, 2019.

717 Zhang, L., Wang, T., Zhang, Q., Zheng, J. Y., Xu, Z., and Lv, M. Y.: Potential sources of nitrous acid (HONO) and their  
718 impacts on ozone: A WRF-Chem study in a polluted subtropical region, *J. Geophys. Res.-Atmos.*, 121, 3645-3662,  
719 10.1002/2015jd024468, 2016.

720 Zhang, L., Li, Q. Y., Wang, T., Ahmadov, R., Zhang, Q., Li, M., and Lv, M. Y.: Combined impacts of nitrous acid and nitryl  
721 chloride on lower-tropospheric ozone: new module development in WRF-Chem and application to China, *Atmos. Chem.*  
722 *Phys.*, 17, 9733-9750, 10.5194/acp-17-9733-2017, 2017.

723 Zhang, L., Chen, Y. F., Zhao, Y. H., Henze, D. K., Zhu, L. Y., Song, Y., Paulot, F., Liu, X. J., Pan, Y. P., Lin, Y., and Huang,  
724 B. X.: Agricultural ammonia emissions in China: reconciling bottom-up and top-down estimates, *Atmos. Chem. Phys.*,  
725 18, 339-355, 10.5194/acp-18-339-2018, 2018.

726 Zhang, Q., Streets, D. G., Carmichael, G. R., He, K. B., Huo, H., Kannari, A., Klimont, Z., Park, I. S., Reddy, S., Fu, J. S.,  
727 Chen, D., Duan, L., Lei, Y., Wang, L. T., and Yao, Z. L.: Asian emissions in 2006 for the NASA INTEX-B mission,  
728 *Atmos. Chem. Phys.*, 9, 5131-5153, 10.5194/acp-9-5131-2009, 2009.

729 Zhang, Q., Pan, Y., He, Y., Zhao, Y., Zhu, L., Zhang, X., Xu, X., Ji, D., Gao, J., Tian, S., Gao, W., and Wang, Y.: Bias in  
730 ammonia emission inventory and implications on emission control of nitrogen oxides over North China Plain, *Atmos.*  
731 *Environ.*, 214, 116869, <https://doi.org/10.1016/j.atmosenv.2019.116869>, 2019.

732 Zhao, Y., Zhou, Y. D., Qiu, L. P., and Zhang, J.: Quantifying the uncertainties of China's emission inventory for industrial  
733 sources: From national to provincial and city scales, *Atmos. Environ.*, 165, 207-221, 10.1016/j.atmosenv.2017.06.045,  
734 2017.

735 Zheng, B., Zhang, Q., Zhang, Y., He, K. B., Wang, K., Zheng, G. J., Duan, F. K., Ma, Y. L., and Kimoto, T.: Heterogeneous  
736 chemistry: a mechanism missing in current models to explain secondary inorganic aerosol formation during the January  
737 2013 haze episode in North China, *Atmos. Chem. Phys.*, 15, 2031-2049, 10.5194/acp-15-2031-2015, 2015.

738 Zheng, B., Chevallier, F., Ciais, P., Yin, Y., Deeter, M. N., Worden, H. M., Wang, Y. L., Zhang, Q., and He, K. B.: Rapid  
739 decline in carbon monoxide emissions and export from East Asia between years 2005 and 2016, *Environ. Res. Lett.*, 13,  
740 9, 10.1088/1748-9326/aab2b3, 2018.

741 Zheng, B., Chevallier, F., Yin, Y., Ciais, P., Fortems-Cheiney, A., Deeter, M. N., Parker, R. J., Wang, Y. L., Worden, H. M.,  
742 and Zhao, Y. H.: Global atmospheric carbon monoxide budget 2000-2017 inferred from multi-species atmospheric  
743 inversions, *Earth Syst. Sci. Data*, 11, 1411-1436, 10.5194/essd-11-1411-2019, 2019.

744 Zhong, L. J., Louie, P. K. K., Zheng, J. Y., Wai, K. M., Ho, J. W. K., Yuan, Z. B., Lau, A. K. H., Yue, D. L., and Zhou, Y.:  
745 The Pearl River Delta Regional Air Quality Monitoring Network - Regional Collaborative Efforts on Joint Air Quality  
746 Management, *Aerosol Air Qual. Res.*, 13, 1582-U1232, 10.4209/aaqr.2012.10.0276, 2013.

747 Zhong, Q. R., Huang, Y., Shen, H. Z., Chen, Y. L., Chen, H., Huang, T. B., Zeng, E. Y., and Tao, S.: Global estimates of  
748 carbon monoxide emissions from 1960 to 2013, *Environ. Sci. Pollut. Res.*, 24, 864-873, 10.1007/s11356-016-7896-2,  
749 2017.

750

## 751 Tables

752 Table 1: Basic configurations of participating models in MICS-Asia III

No	Horizontal resolution	Vertical resolution	First layer height	Horizontal advection	Vertical advection	Horizontal Diffusion	Vertical Diffusion	Gas phase chemistry	Aerosol processes	Dry deposition of gases	Wet deposition of gases	Meteorology	Boundary condition	Online (Yes or No)
M1	45km	40 $\sigma_p$ level	57 m	Yamo (Yamartino, 1993)	ppm (Collella and Woodward, 1984)	multiscale	ACM2 (Pleim, 2007)	SAPRC99 (Carter, 2000)	Aero6 (Binkowski and Roselle, 2003)	Wesely (1989)	Henry's law	Standard <sup>a</sup>	GEOS-Chem (Martin et al., 2002)	No
M2	45km	40 $\sigma_p$ level	57 m	Yamo	ppm	multiscale	ACM2	SAPRC99	Aero6	Wesely (1989)	Henry's law	Standard <sup>a</sup>	Default	No
M3	45km	40 $\sigma_p$ level	57 m	Yamo	Yamo	multiscale	ACM2	CB05 (Yarwood et al., 2005)	Aero5	Wesely (1989)	Henry's law	Standard <sup>a</sup>	GEOS-Chem	No
M4	45km	40 $\sigma_p$ level	57 m	ppm	ppm	multiscale	ACM2_ inline	SAPRC99	Aero5	Wesely (1989)	Henry's law	Standard <sup>a</sup>	CHASER (Sudo et al., 2002a)	No
M5	45km	40 $\sigma_p$ level	57 m	ppm	ppm	multiscale	ACM2_ inline	SAPRC99	Aero5	M3DRY (Pleim et al., 2001)	Henry's law	Standard <sup>a</sup>	CHASER	No
M6	45km	40 $\sigma_p$ level	57 m	Yamo	Yamo	multiscale	ACM2_ inline	SAPRC99	Aero5	M3DRY	ACM	Standard <sup>a</sup>	CHASER	No
M7	45km	40 $\sigma_p$ level	29 m	WRF	5 <sup>th</sup> order Monotonic	WRF	3 <sup>rd</sup> order Monotonic	RACM-ESRL with KPP (Goliff et al., 2013)	MADE (Ackerman et al., 1998)	Wesely (1989)	Henry's law	WRF/NCEP <sup>a</sup>	Default	No
M8	45km	40 $\sigma_p$ level	57 m	5 <sup>th</sup> order Monotonic	3 <sup>rd</sup> order Monotonic	MYJ	MYJ	RACM with KPP	MADE	Wesely (1989)	AQCHEM	WRF/NCEP <sup>a</sup>	CHASER	Yes
M9	45km	40 $\sigma_p$ level	16 m	5 <sup>th</sup> order Monotonic	3 <sup>rd</sup> order Monotonic	Smagorinsky first order closure	YSU (Hong et al., 2006)	RADM2 (Stockwell et al., 1990)	MADE	Wesely (1989)	Easter et al., (2004)	WRF/NCEP <sup>a</sup>	GEOS-Chem	Yes
M10	45km	60 $\sigma_p$ level	44 m	Monotonic	3 <sup>rd</sup> order Monotonic	2 <sup>nd</sup> order Monotonic	YSU	RADM2	GOCART	Wesely (1989)	Grell	WRF/MERRA2 <sup>a</sup>	MOZART + GOCART <sup>b</sup>	No
M11	45km	20 $\sigma_z$ level	50 m	Walcek and Aleksic (1998)	Walcek and Aleksic (1998)	multiscale	K-theory	CBMZ (Zaveri et al., 1999)	ISORROPI A1.7 (Nenes et al., 1998)	Wesely (1989)	Henry's law	Standard <sup>a</sup>	CHASER	No



M12	45km	40 $\sigma_p$ level	54 m	Walcek and Aleksic (1998)	Walcek and Aleksic (1998)	FTCS	FTCS	SAPRC99	Kajino et al. (2012)	Zhang et al. (2003)	Henry's law	Standard <sup>a</sup>	CHASER	No
M13	0.5°×0.667°	47 $\sigma_p$ level	60 m	ppm	ppm	Lin and McElroy, 2010	Lin and McElroy, 2010	NO <sub>x</sub> -O <sub>3</sub> -HC	ISORROPI A2.0 (Fountoukis and Nenes, 2007)	Wesely	Henry's law	GEOS-5 <sup>a</sup>	Geos-Chem	No
M14	64km	15 $\sigma_z$ level	100 m	ppm	ppm	multiscale	ACM2	SAPRC99	ISORROPI A1.7	Wesely (1989)	Henry's law	RAMS/NCEP <sup>a</sup>	Geos-Chem	No

753

754 <sup>a</sup> Standard represents the reference meteorological field provided by MICS-Asia III project; WRF/NCEP and WRF/MERRA represents the meteorological field of the participating model itself, which was run by WRF driven by the NCEP and  
755 Modern Era Retrospective-analysis for Research and Applications (MERRA) reanalysis dataset. RAMS/NCEP is the meteorology field run by RAMS driven by the NCEP reanalysis dataset.

756 <sup>b</sup> Boundary conditions of M10 are from MOZART and GOCART (Chin et al., 2002; Horowitz et al., 2003), which provided results for gaseous pollutants and aerosols, respectively.

757

758

759

760

761

762

763

764

765

766

767

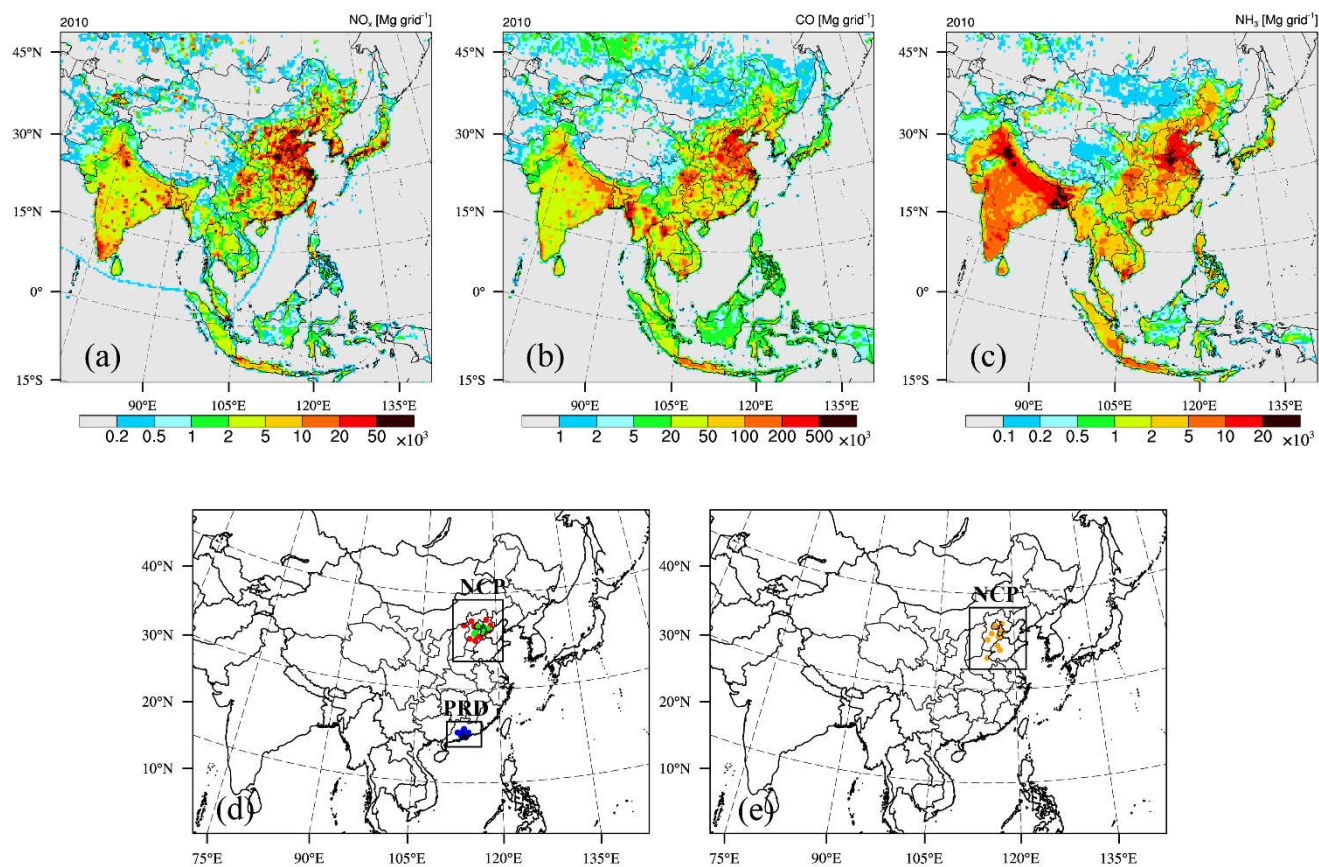
768 **Table 2: Statistics of simulated annual mean concentrations over the NCP and PRD regions.**

Species	Regions	Statistics	Model													
			M1	M2	M4	M5	M6	M7	M8	M9	M10	M11	M12	M13	M14	Ense
NO <sub>2</sub>	NCP	R(spatial) <sup>a</sup>	0.63	0.67	0.67	0.67	0.67	0.70	0.70	0.59	0.57	0.66	0.69	-	0.70	0.67
		R(temporal) <sup>b</sup>	0.82	0.92	0.93	0.86	0.92	0.81	0.28	0.85	0.95	0.75	0.90	-	0.96	0.91
		MBE	-4.11	-5.66	-6.54	1.86	-5.12	-5.04	3.30	8.28	-2.45	0.00	-3.81	-	-2.99	-1.86
		NMB(%)	-17.8	-24.5	-28.4	8.0	-22.2	-21.9	14.2	35.9	-10.6	0.02	-16.5	-	-13.0	-8.0
		RMSE	7.40	8.25	8.79	6.75	8.01	7.55	6.54	12.74	7.72	6.37	7.38	-	6.68	6.36
	PRD	R(spatial) <sup>a</sup>	0.12	0.06	0.07	0.07	0.06	0.12	0.20	0.38	0.00	0.08	0.12	-	0.02	0.10
		R(temporal) <sup>b</sup>	0.93	0.80	0.86	0.88	0.79	0.68	0.83	0.95	0.74	0.74	0.75	-	0.52	0.86
		MBE	-6.73	-9.84	-7.21	1.96	-6.66	-3.99	3.24	-7.61	-1.84	3.02	-5.49	-	-5.03	-3.85
		NMB(%)	-30.1	-44.0	-32.3	8.8	-29.8	-17.9	14.5	-34.0	-8.2	13.5	-24.6	-	-22.5	-17.2
		RMSE	11.31	13.14	12.00	10.80	11.84	10.60	8.73	10.69	10.72	10.51	11.68	-	12.00	10.15
CO	NCP	R(spatial) <sup>a</sup>	0.35	0.48	0.27	0.34	0.36	0.22	0.19	0.48	0.49	0.33	0.35	-0.13	0.29	0.37
		R(temporal) <sup>b</sup>	0.94	0.96	0.92	0.22	0.90	0.77	0.94	0.92	0.82	0.85	0.94	0.85	0.88	0.92
		MBE	-1.53	-1.35	-1.59	-1.69	-1.52	-1.64	-1.29	-1.16	-1.55	-1.37	-1.38	-1.53	-1.51	-1.47
		NMB(%)	-68.9	-60.9	-71.4	-76.2	-68.2	-73.7	-58.2	-52.0	-70.0	-61.6	-62.3	-68.9	-68.0	-66.2
		RMSE	1.71	1.54	1.77	1.86	1.70	1.82	1.51	1.36	1.74	1.57	1.58	1.74	1.70	1.66
	PRD	R(spatial) <sup>a</sup>	0.04	-0.24	-0.25	-0.23	-0.22	-0.05	0.08	0.55	-0.02	-0.01	-0.22	0.09	-0.21	-0.06
		R(temporal) <sup>b</sup>	0.96	0.91	0.93	0.84	0.95	0.90	0.90	0.96	0.83	0.87	0.93	0.76	0.82	0.94
		MBE	-0.66	-0.64	-0.65	-0.64	-0.62	-0.64	-0.51	-0.57	-0.50	-0.51	-0.58	-0.52	-0.67	-0.59
		NMB(%)	-68.4	-67.0	-67.0	-66.7	-64.7	-66.5	-53.3	-59.7	-52.3	-52.7	-60.7	-54.1	-69.6	-61.7
		RMSE	0.70	0.70	0.70	0.69	0.67	0.69	0.57	0.62	0.56	0.57	0.64	0.58	0.72	0.65
NH <sub>3</sub>	NCP	R(spatial) <sup>a</sup>	0.72	0.70	0.69	0.70	0.71	0.65	-	0.70	0.57	0.62	0.67	0.61	0.58	0.69
		R(temporal) <sup>b</sup>	-0.48	-0.22	-0.45	-0.55	-0.41	0.04	-	-0.19	0.64	0.08	-0.37	0.65	-0.04	-0.17
		MBE	-0.69	2.95	-6.14	-6.61	-3.89	4.94	-	21.8	10.5	-0.07	0.31	-5.19	-12.2	0.47
		NMB(%)	-3.8	16.1	-33.5	-36.0	-21.2	26.9	-	118.7	57.1	-0.4	1.69	-28.3	-66.3	2.59
		RMSE	7.20	10.04	8.95	9.24	7.48	8.78	-	29.24	13.48	8.30	7.33	8.82	14.48	7.20

769 <sup>a</sup> R(spatial) represents the spatial correlation coefficients between simulated and observed concentrations sampled from different stations in the NCP and PRD regions;

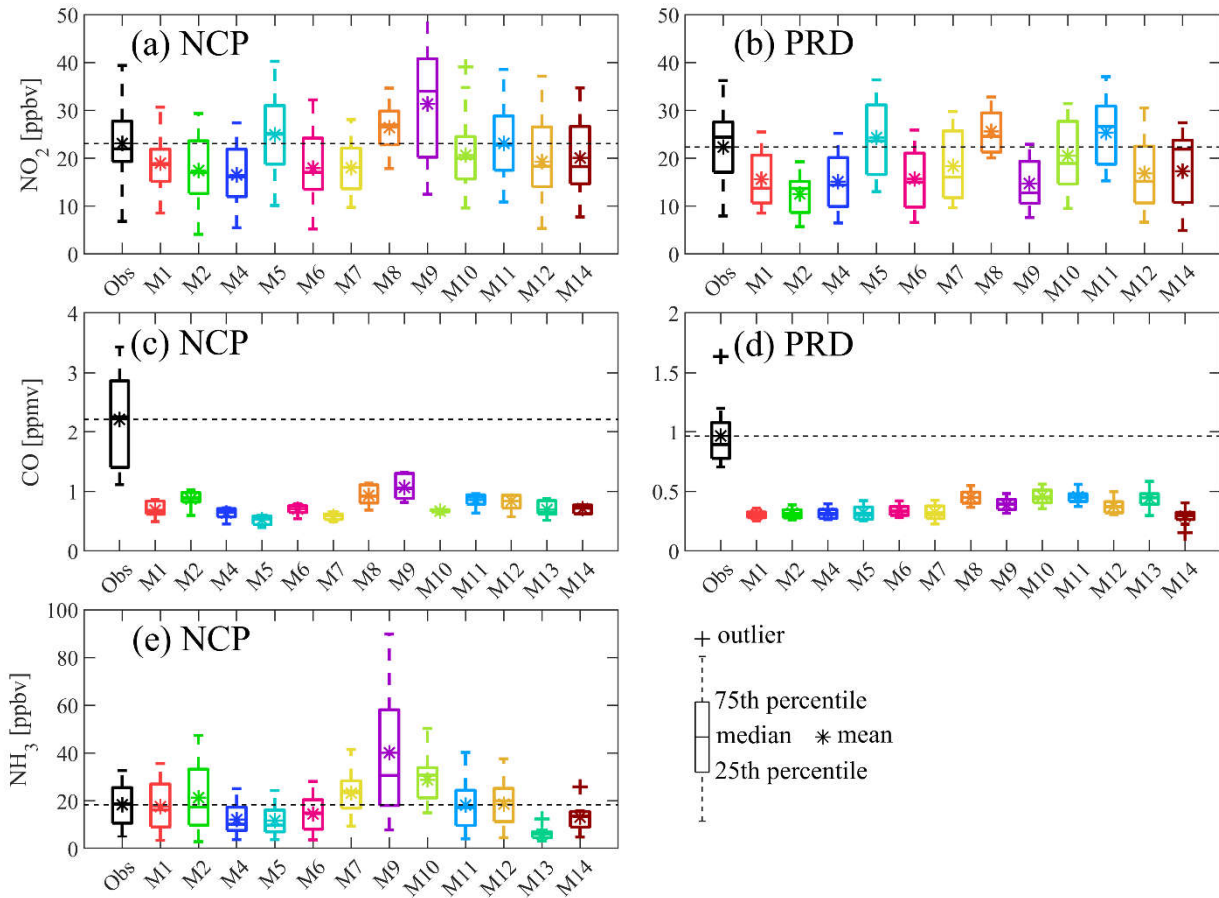
770 <sup>b</sup> R(temporal) represents the temporal correlation coefficients between simulated and observed monthly mean concentrations from January to December in 2010;

771



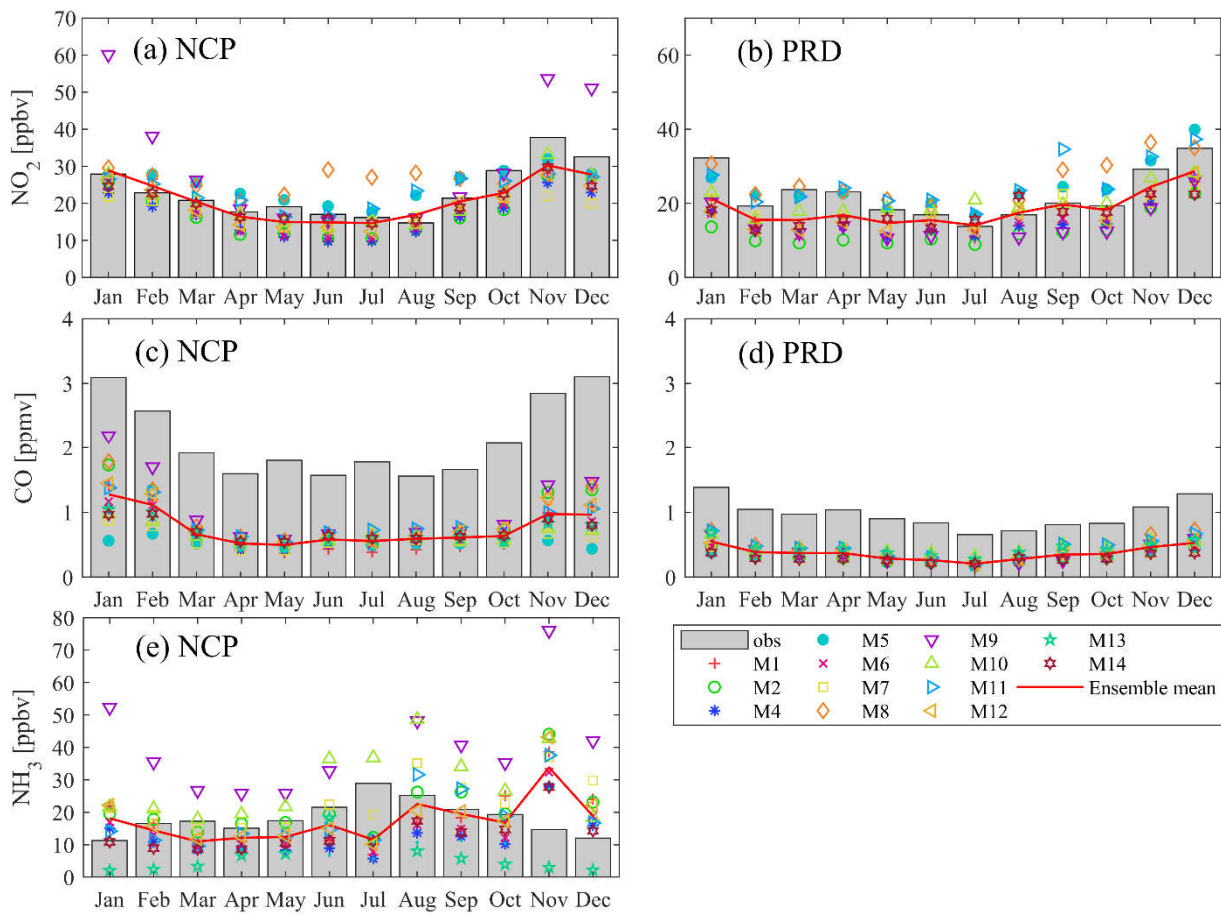
773

774 **Figure 1: Modeling domains of the participated models except M13 and M14 along with spatial distributions of the total emissions**  
 775 **of (a) NO<sub>x</sub>, (b) CO and (c) NH<sub>3</sub> in 2010 provided by MICS-Asia III (upper panel), and the distributions of observation stations of (d)**  
 776 **NO<sub>2</sub> and CO over the NCP and PRD regions, as well as (e) NH<sub>3</sub> over the NCP region (lower panel). The horizontal resolution is**  
 777 **45km×45km. Note that domains of M13 and M14 are shown in fig. 7 and only six of nineteen observational sites (green) over the**  
 778 **NCP region have CO measurements.**



779

780 **Figure 2: Boxplot of simulated and observed annual mean NO<sub>2</sub>, CO and NH<sub>3</sub> concentrations sampled from different stations over**  
 781 **the NCP (a, c, e) and PRD (b, d) regions. The outlier was defined as values larger than  $q_3 + 1.5 \times (q_3 - q_1)$  or less than  $q_1 -$**   
 782  **$1.5 \times (q_3 - q_1)$ , where  $q_3$  denotes the 75th percentile, and  $q_1$  the 25th percentile. This approximately corresponds to 99.3 percent**  
 783 **coverage if the data are normally distributed.**



784

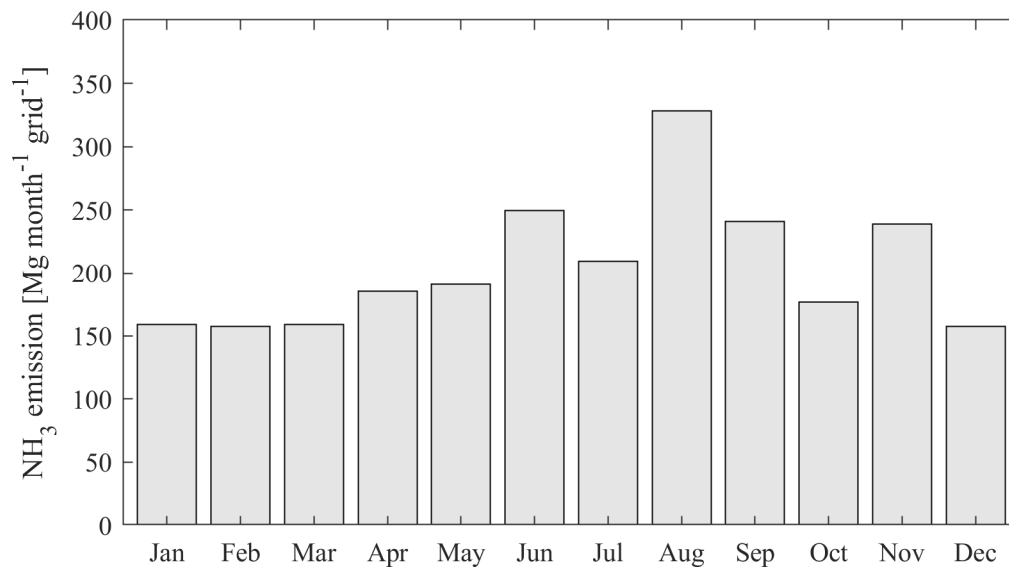
785 **Figure 3: Timeseries of regional mean  $\text{NO}_2$ , CO concentrations over the NCP (a, c) and PRD (b, d) regions as well as  $\text{NH}_3$**   
 786 **concentrations over the NCP (e) region from January to December in year 2010.**

787

788

789

790



791

792 **Figure 4: Timeseries of NH<sub>3</sub> emissions over the NCP region provided by MICS-Asia III on a horizontal resolution of 45km from**  
 793 **January to December in year 2010.**

794

795

796

797

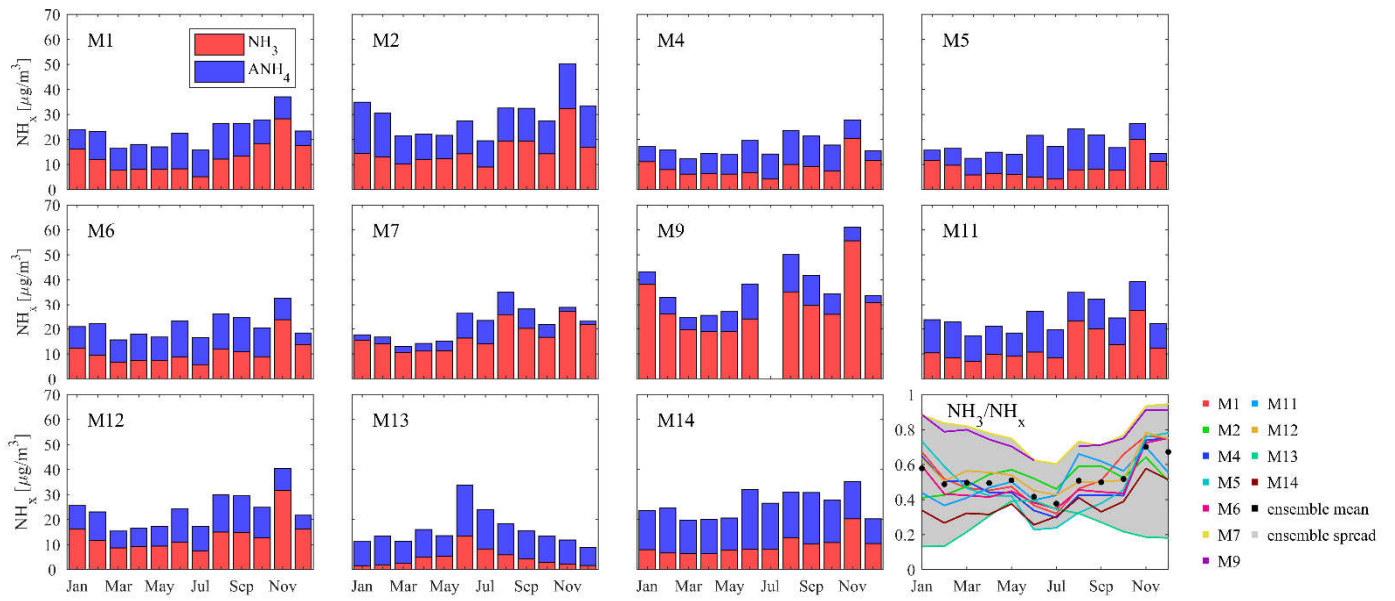
798

799

800

801

802



803

804 **Figure 5: Timeseries of the multi-model simulated total ammonium ( $\text{NH}_x = \text{NH}_3 + \text{NH}_4^+$ ) in atmosphere along with the ratio of**  
 805 **gaseous  $\text{NH}_3$  to the total ammonium over the NCP region from January to December in year 2010.**

806

807

808

809

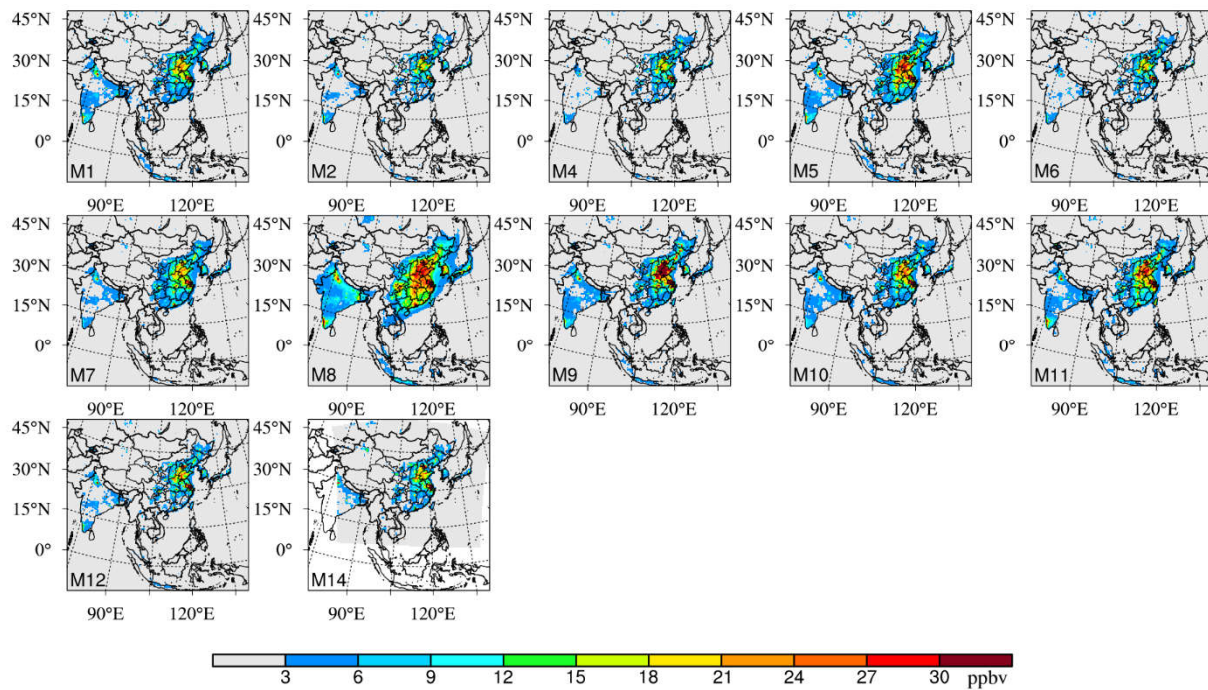
810

811

812

813

814



815

816 **Figure 6: Spatial distribution of the annual mean NO<sub>2</sub> concentrations from each modeling results of MICS-Asia III. Note that M13**  
 817 **are not included in this figure.**

818

819

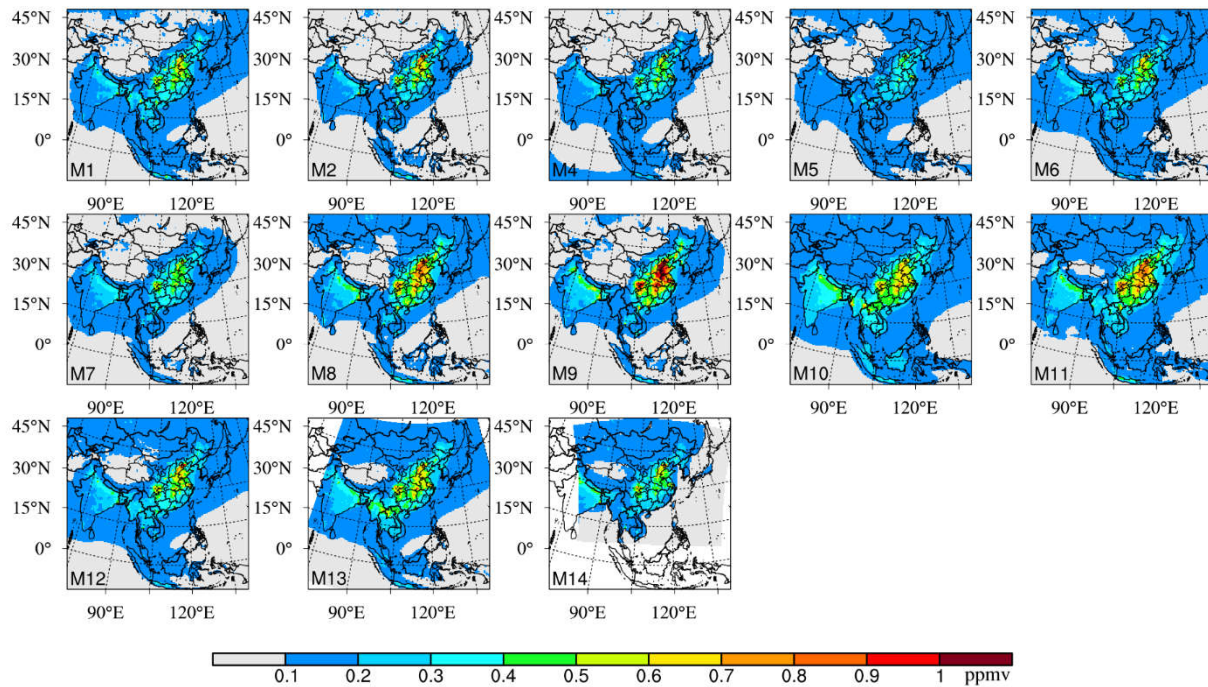
820

821

822

823





824

825 **Figure 7: Spatial distribution of the annual mean CO concentrations from each modeling results of MICS-Asia III.**

826

827

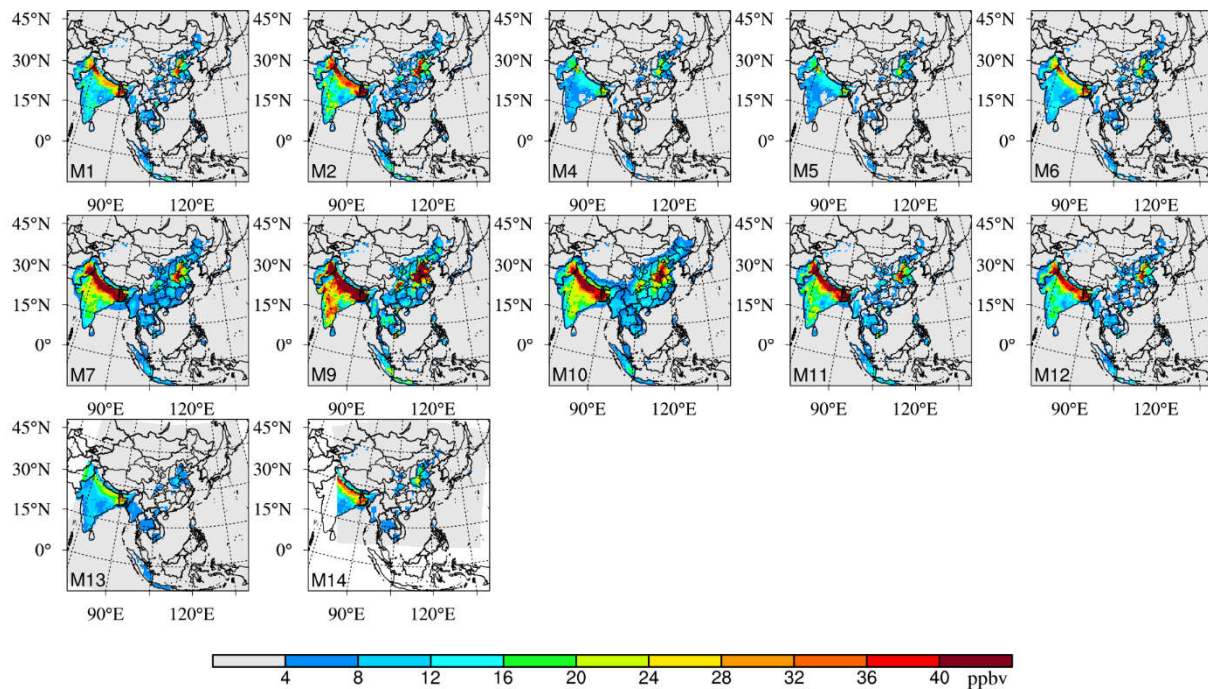
828

829

830

831

832



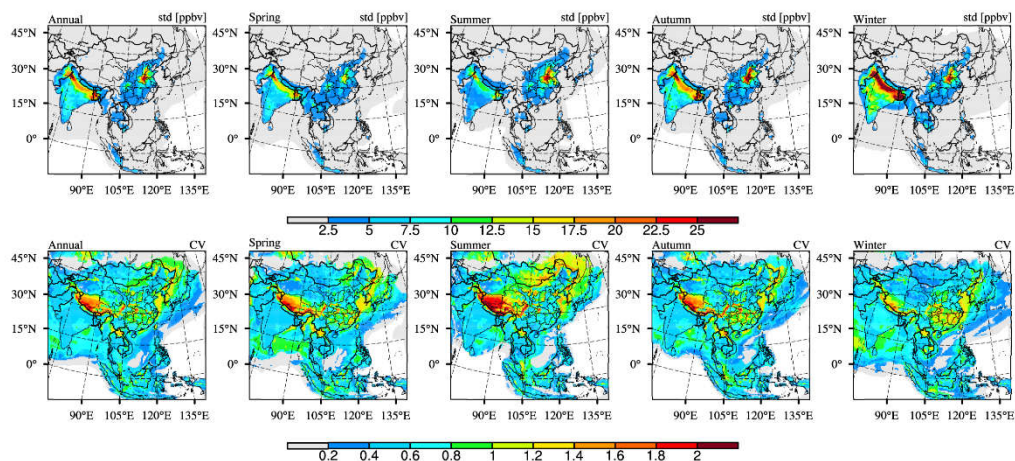
833

834 **Figure 8: Spatial distribution of the annual mean  $\text{NH}_3$  concentrations from each modeling results of MICS-Asia III.**

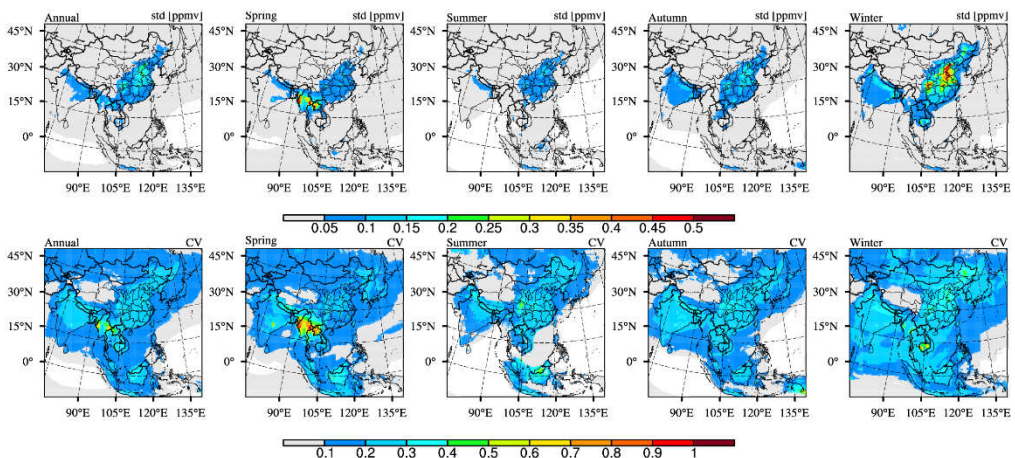
835



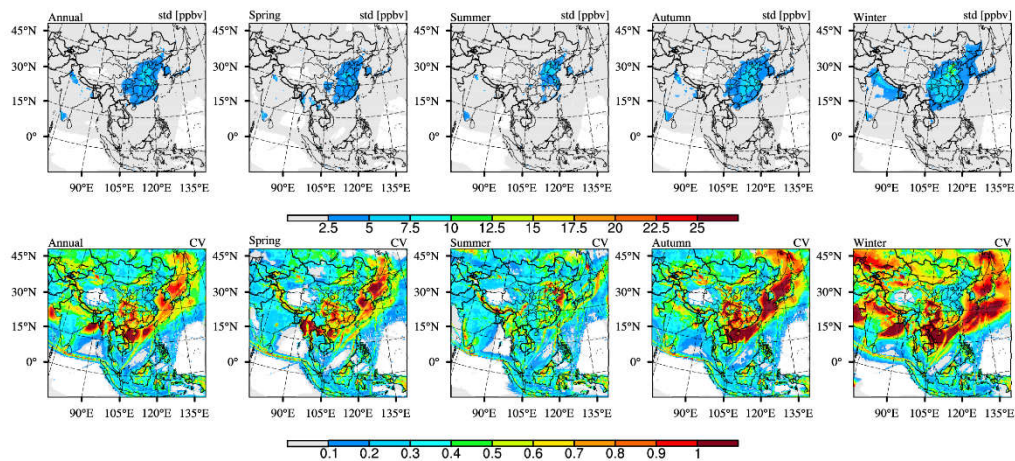
(a)  $\text{NH}_3$ :



(b) CO:



(c)  $\text{NO}_2$ :



836

837 **Figure 9: Spatial distribution of the standard deviation of (a)  $\text{NH}_3$ , (b) CO and (c)  $\text{NO}_2$  multi-model predictions from MICS-Asia III,**  
838 **as well as the corresponding distribution of CV on the annual and seasonal basis.**